VORTEX EVOLUTION

IN REALISTIC GEOPHYSICAL FLOWS

by
Donald P. Delisi
and
Robert E. Robins

19970513 062

DISCLAIMER NOTICE

UNCLASSIFIED

Technical Report
distributed by

**DEFENSE
TECHNICAL
INFORMATION
CENTER**

DTIC

UNCLASSIFIED

THIS DOCUMENT IS BEST
QUALITY AVAILABLE. THE
COPY FURNISHED TO DTIC
CONTAINED A SIGNIFICANT
NUMBER OF PAGES WHICH DO
NOT REPRODUCE LEGIBLY.

NWRA-CR-93-R083

8 July 1996

VORTEX EVOLUTION

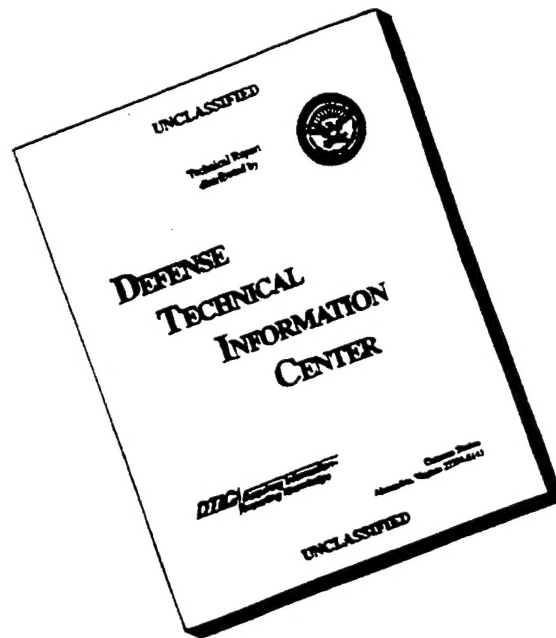# IN REALISTIC GEOPHYSICAL FLOWS

by
Donald P. Delisi
and
Robert E. Robins

REPORT DOCUMENTATION PAGE

Public reporting burden for this collection of information is estimated to average 1 hour per response, including the time for reviewing instructions, searching existing data sources, gathering and maintaining the data needed, and completing and reviewing the collection of information. Send comments regarding this burden estimate or another aspect of this collection of information, including suggestions for reducing this burden, to Washington Headquarters Services, Directorate for Information Operations and Reports, 1215 Jefferson Davis Highway, Suite 1204, Arlington, VA 22202-4302, and to the Office of Management and Budget, Paperwork Reduction Project (0704-0188), Washington, DC 20503.

1. AGENCY USE ONLY *(Leave blank)*	2. REPORT DATE 8 July 1996	3. REPORT TYPE AND DATES COVERED Final Report, 01 Jan 89 - 31 Dec 91

4. TITLE AND SUBTITLE Vortex Evolution in Realistic Geophysical Flows	5. FUNDING NUMBERS N00014-89-C-0030

6. AUTHOR(S)

Donald P. Delisi

Robert E. Robins

7. PERFORMING ORGANIZATION NAME(S) AND ADDRESS(ES) Northwest Research Associates, Inc. 300 120th Ave NE, Bldg 7, Ste 220 P.O. Box 3027 Bellevue, WA 98009-3027	8. PERFORMING ORGANIZATION REPORT NUMBER NWRA-CR-93-R083

9. SPONSORING / MONITORING AGENCY NAME(S) AND ADDRESS(ES) Office of Naval Research 800 North Quincy Street Arlington, VA 22217	10. SPONSORING / MONITORING AGENCY REPORT NUMBER

11. SUPPLEMENTARY NOTES

12a. DISTRIBUTION / AVAILABILITY STATEMENT	12b. DISTRIBUTION CODE

13. ABSTRACT (Maximum 200 words)

Laboratory experiments and numerical simulations of vortex evolution in realistic geophysical flows are reported. Two laboratory experiments are discussed. The first experiment examined three-dimensional vortices produced from a wing in a nonstratified nonsheared flow. This study showed that vortices can migrate farther and last longer than previously reported. The second laboratory experiment investigated the evolution of two-dimensional vortices in a stratified shear flow. This experiment showed the evolution of a "solitary" vortex when the background Richardson number was around four or less. Circulation estimates were also obtained for these vortices and showed a more rapid decay of circulation of the countersign vortex.

Two numerical studies are also reported. In the first numerical study, we examined the evolution of a two-dimensional vortex pair in a stratified shear flow. This study showed that the vortex pair evolved into a solitary vortex when the ambient Richardson number was on the order of unity or less. A second numerical study used a k-ε model to examine the evolution of a two-dimensional vortex pair. It was found that the standard k-ε model did a poor job of representing the turbulent dissipation in vortex flows. Good agreement with experimental results was obtained with this model with a reduction in the eddy viscosity coefficient.

14. SUBJECT TERMS vortex, stratification, shear, Richardson number, laboratory, numerical	15. NUMBER OF PAGES
	16. PRICE CODE

17. SECURITY CLASSIFICATION OF REPORT Unclassified	18. SECURITY CLASSIFICATION OF THIS PAGE Unclassified	19. SECURITY CLASSIFICATION OF ABSTRACT Unclassified	20. LIMITATION OF ABSTRACT

Table of Contents

List of Figures

1. Background

This report is the Final Report for contract N00014-89-C-0030 from the Office of Naval Research to Northwest Research Associates, Inc. (NWRA) for Studies of Vortex Evolution in Realistic Fluids. The period of performance for this contract was 1 January 1989 to 31 December 1991. The contract monitor was Dr. Edwin P. Rood.

2. Introduction

Any lifting surface, such as a wing at an angle of attack, will generate vorticity. This vorticity is shed behind the lifting surface, and typically rolls up rapidly into a vortex pair. Our recent studies on the measurement and prediction of the migration and evolution of this vortex pair in realistic environments are the subject of this report.

There have been many previous experimental, numerical, and theoretical studies of vortex evolution. For some of the many reviews available, see Hall (1972), Widnall (1975), Leibovich (1978), Saffman and Baker (1979), Smith (1986), and Sarpkaya (1989). Despite this extensive research, our understanding is far from complete. This lack of understanding is due, at least in part, to the complexity of vortex flows. For example, real-world vortices have high Reynolds numbers and are turbulent, highly rotational flows far from solid boundaries. Any one of these elements by themselves is difficult to understand and predict; taken together, they represent very challenging fluid mechanics.

Most previous studies of vortex evolution have examined flows in relatively simple backgrounds. For example, experimental studies have been performed in nonstratified and nonsheared backgrounds (Barker and Crow, 1977) and in stratified and nonsheared backgrounds (Tomassian, 1979; Sarpkaya 1983), but not in backgrounds with both stratification and shear. Similarly, numerical studies have been performed in a nonstratified, sheared background (Bilanin et al, 1978) but have not been performed in backgrounds with both stratification and shear.

This lack of knowledge of background effects on vortices is particularly important for the Navy, since oceanic measurements indicate that both stratification and shear are typically present in the ocean. The Richardson number, Ri, defined as the ratio of stratification, or buoyancy, forces to shear, or inertial, forces is given by

$$Ri = N^2 / U_z^2 \qquad (1)$$

where N is the Brunt-Vaisala (B-V) frequency defined by

$$N = \left[-\frac{g}{\overline{\rho}} \frac{d\rho}{dz} \right]^{\frac{1}{2}} \qquad (2)$$

where g is the acceleration due to gravity; ρ is density; $\overline{\rho}$ is average density; z is the vertical coordinate; and the shear, U_z, is the vertical derivative of the horizontal speed of the fluid.

Measurements of Richardson number in the ocean indicate that the number is typically below four and is usually near one (Evans, 1982; Toole and Hayes, 1984). Thus, in the ocean, shear forces are of the same order of magnitude as stratification forces. It is well known that stratification and shear acting separately have important effects on vortex evolution (Tomassian, 1979; Sarpkaya, 1983; Bilanin et al, 1978). We will show below that stratification and shear acting together in flows with the Richardson number near one also have important effects on vortex evolution.

3.   Manuscripts Resulting From This Contract

The following papers resulted from this contract:

Robins, R.E., and Delisi, D.P., 1990. Numerical Study of Vertical Shear and Stratification Effects on the Evolution of a Vortex Pair. *AIAA Journal, 28*, 661-669.

Delisi, D.P., and Greene, G.C., 1990. Measurements and Implications of Vortex Motions Using Two Flow-Visualization Techniques. *Journal of Aircraft, 27*, 968-971.

Delisi, D.P., Robins, R.E., and Lucas, R.D., 1991. Initial Laboratory Observations of the Evolution of a Vortex Pair In a Stratified Shear Flow. *Physics of Fluids A, 3*, 2489-2491.

Delisi, D.P., Robins, R.E., and Altman, D.B., 1991. Laboratory and Numerical Studies of Vortex Evolution in Ideal and Realistic Environments. Proceedings of the Aircraft Wake Vortex Conference, DOT/FAA/SD-92/1.2, 30-1 to 30-28.

4.   Significant Results

This section contains significant results from this contract. The results are presented in the order the papers are listed in Section 3.

4.1. Results from Robins and Delisi, 1990, *AIAA Journal, 28*, 661-669.

This paper reported the first numerical study to show how coexisting stratification and vertical shear affect the evolution of a vortex pair. A two-dimensional, time-dependent, Navier-Stokes numerical model was used to study vortex evolution in a variety of flows. A wave-number-dependent damping was used to prevent the buildup of energy at small scales.

The significant results from this paper are shown in Figures 1 through 10. Figures 1 through 4 show plots for the case of vortex evolution with stratification but no shear (Ri = infinite). In this calculation, the right vortex is rotating clockwise and the left vortex is rotating counterclockwise, resulting in a rising vortex pair. Figure 1 shows contours of perturbation vorticity; Figure 2 shows contours of total density; Figure 3 shows the horizontally summed total, kinetic, and potential perturbation energy density versus height; and Figure 4 shows total, kinetic, and potential perturbation energy versus time. All times shown are non-dimensional, with $t = 2\pi$ corresponding to 1 B-V period. Initially, the vortices rise as time increases, pulling heavy fluid up (frames a to c in Figures 1-3). Around frame d in these figures, this heavy fluid begins to fall. The motion associated with this falling fluid dominates the flow for frames d through f. Note from Figures 1 and 2 that the flow is symmetric, with the left and right vortices decaying at equal rates. From Figure 4, we see that the flow evolves toward equipartition of potential and kinetic energy, as the flow evolves into an internal wave field.

Figures 5 through 8 show the same plots as Figures 1 through 4 for the same vortices, except now a vertical shear has been added to make the Richardson number equal to 0.5. The shear has a clockwise rotation; that is, in the vortex frame of reference, the flow at the top is from left to right, and the flow at the bottom is from right to left. Figures 5 and 6 show that, in this example, the counterclockwise (left) vortex is gradually destroyed, leaving only the clockwise (right) vortex (a "solitary" vortex). The density plots in Figure 6 show an initial upward advection of heavy fluid, but no significant downward advection as seen in the no-shear case. The energy plots in Figure 7 show that the energy-density peak remains high and does not descend as in Figure 3. Finally, Figure 8 shows there is no longer a trend toward equipartition of energy at late times, but rather a dominance of kinetic over potential energy.

Figures 5 to 8 show the dramatic effect of shear on the evolution of a vortex pair in a stratified flow. Without shear, the vortices evolved symmetrically, losing their individual identities equally rapidly. With shear, the vortex with rotation opposite to the rotational sense of the mean shear was destroyed, and the vortex with rotation in the same sense as the mean shear survived. In this case, a solitary vortex was formed, and it decayed slowly with time.
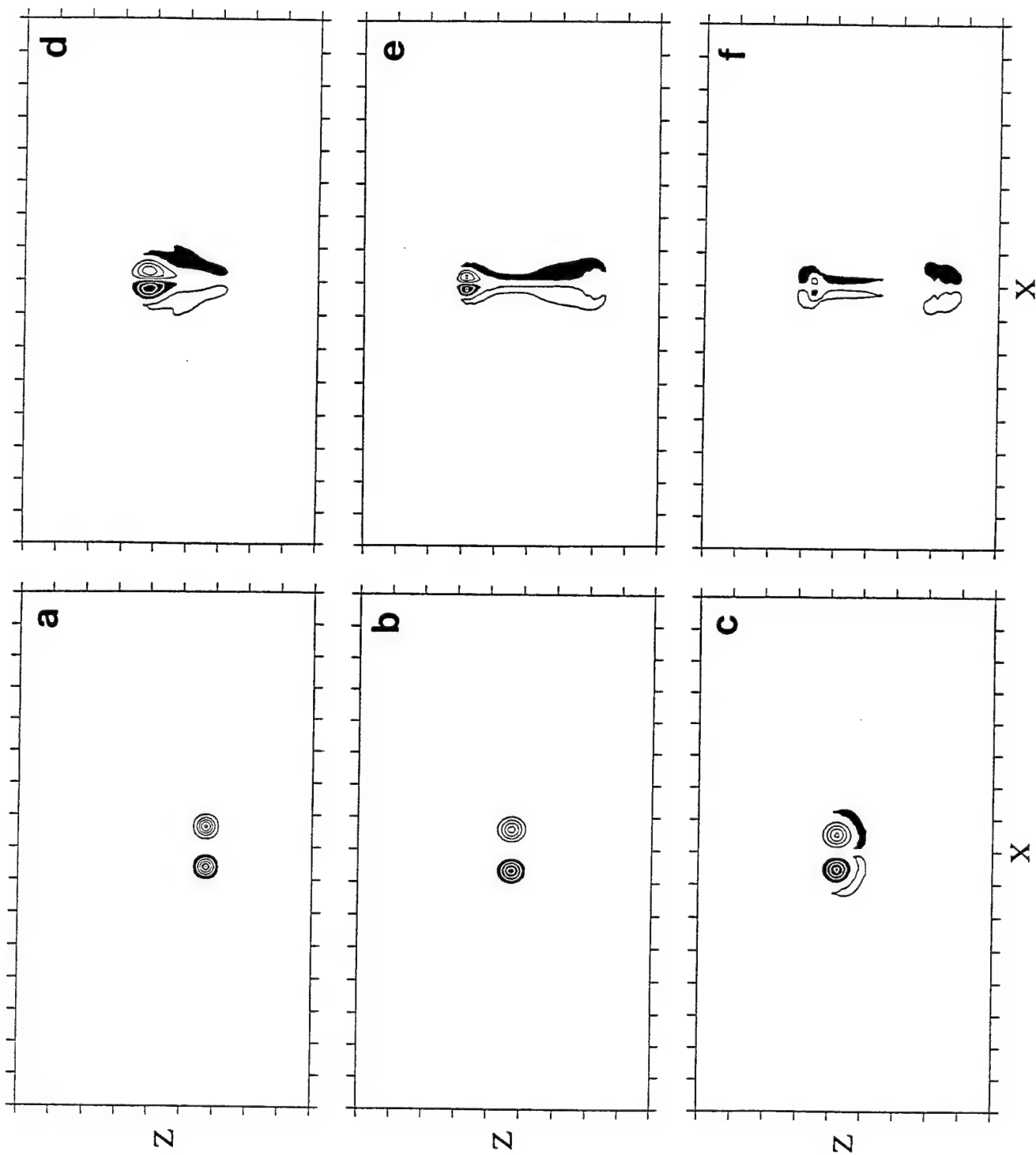
Figure 1. Contours of perturbation vorticity at non-dimensional times 0, 1, 2, 3, 4, and 5 (a through f, respectively), for the no-shear case Ri = ∞ [white (black) shading signifies clockwise (counterclockwise) vorticity].

4
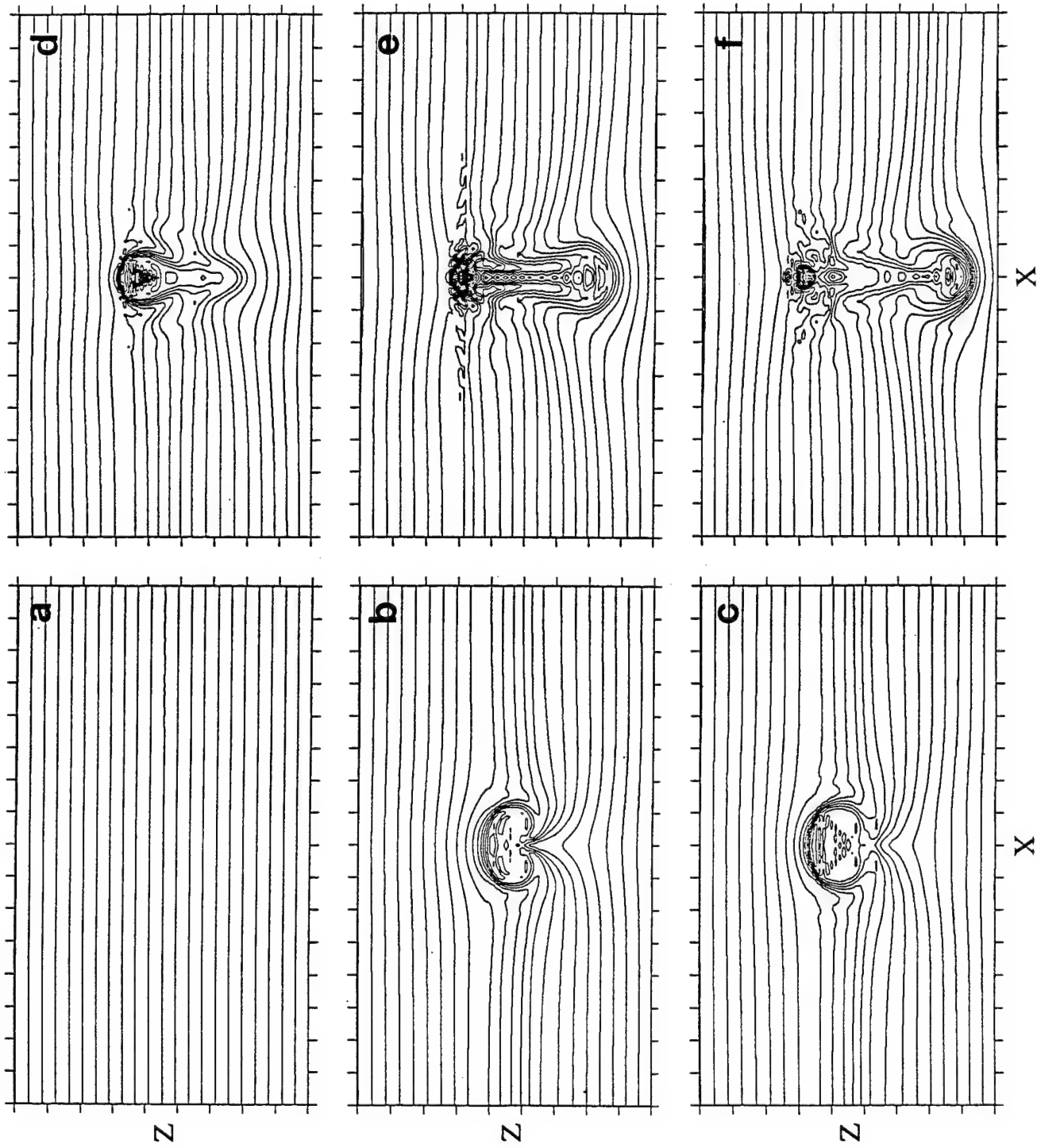
Figure 2.   Contours of total density, $\rho + \rho'$, at non-dimensional times 0, 1, 2, 3, 4 and 5 (a through f, respectively), for the no-shear case Ri = ∞.

5
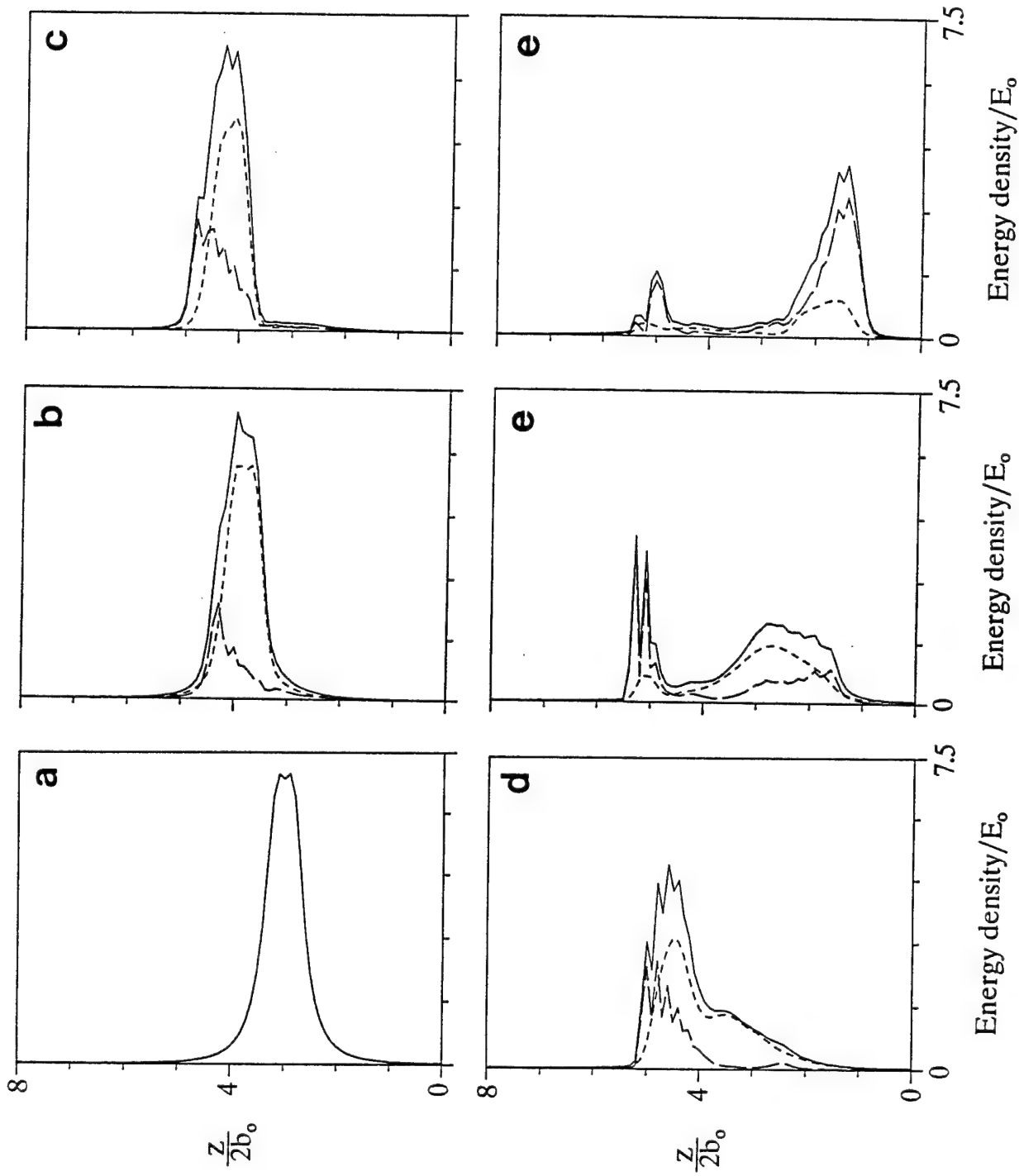
Figure 3. Vertical profiles of horizontally summed perturbation energy density for non-dimensional times 0, 1, 2, 3, 4 and 5 (a through f, respectively), for the no-shear case $Ri = \infty$ (solid, short-dash, and long-dash lines signify total, kinetic, and potential perturbation energy density, respectively).
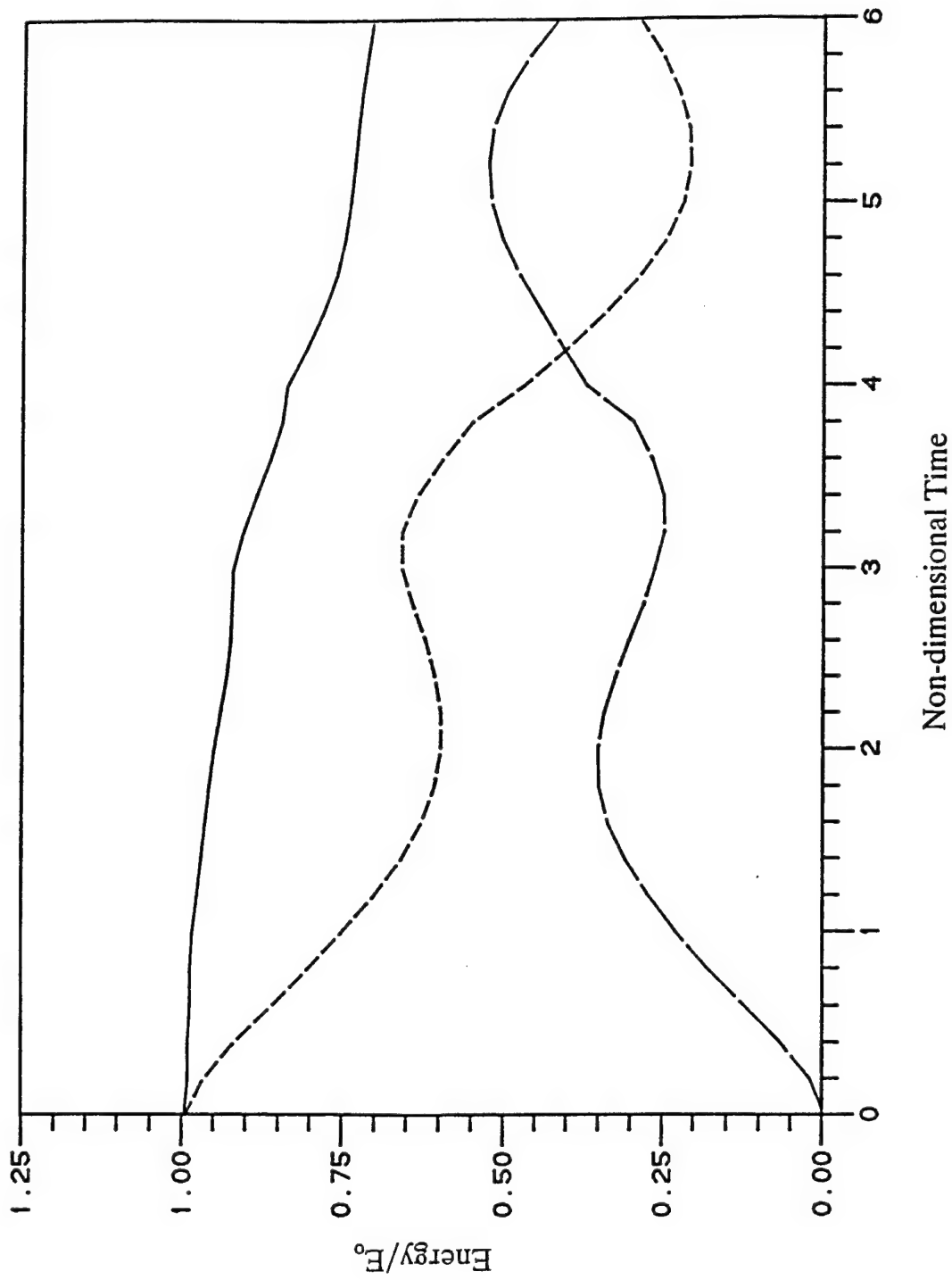
Figure 4. Perturbation energy versus time for the no-shear case Ri = ∞ (solid, short-dash, and long-dash lines signify total, kinetic, and potential perturbation energy, respectively).
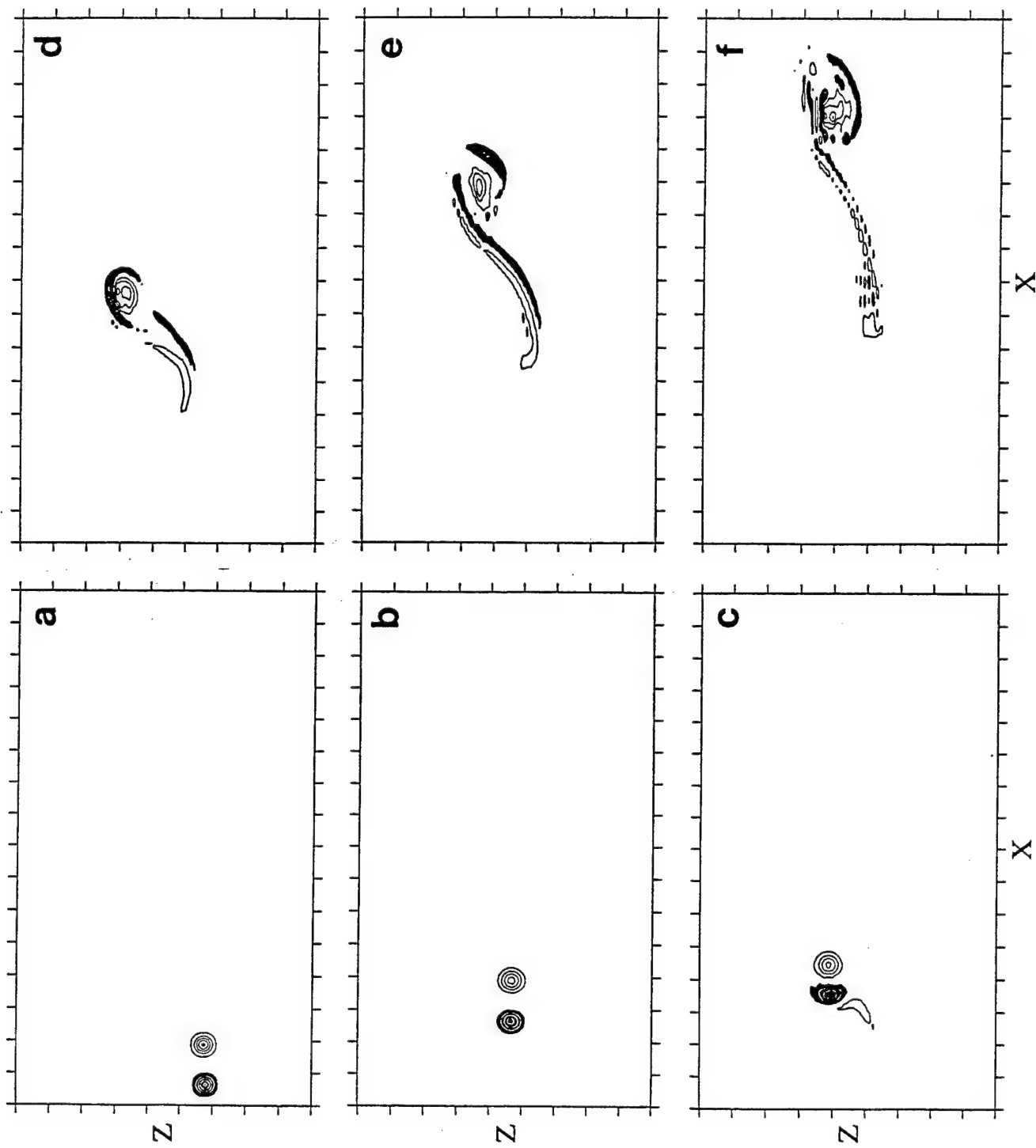
Figure 5.   As in Figure 1 for the case Ri = 0.5.

8
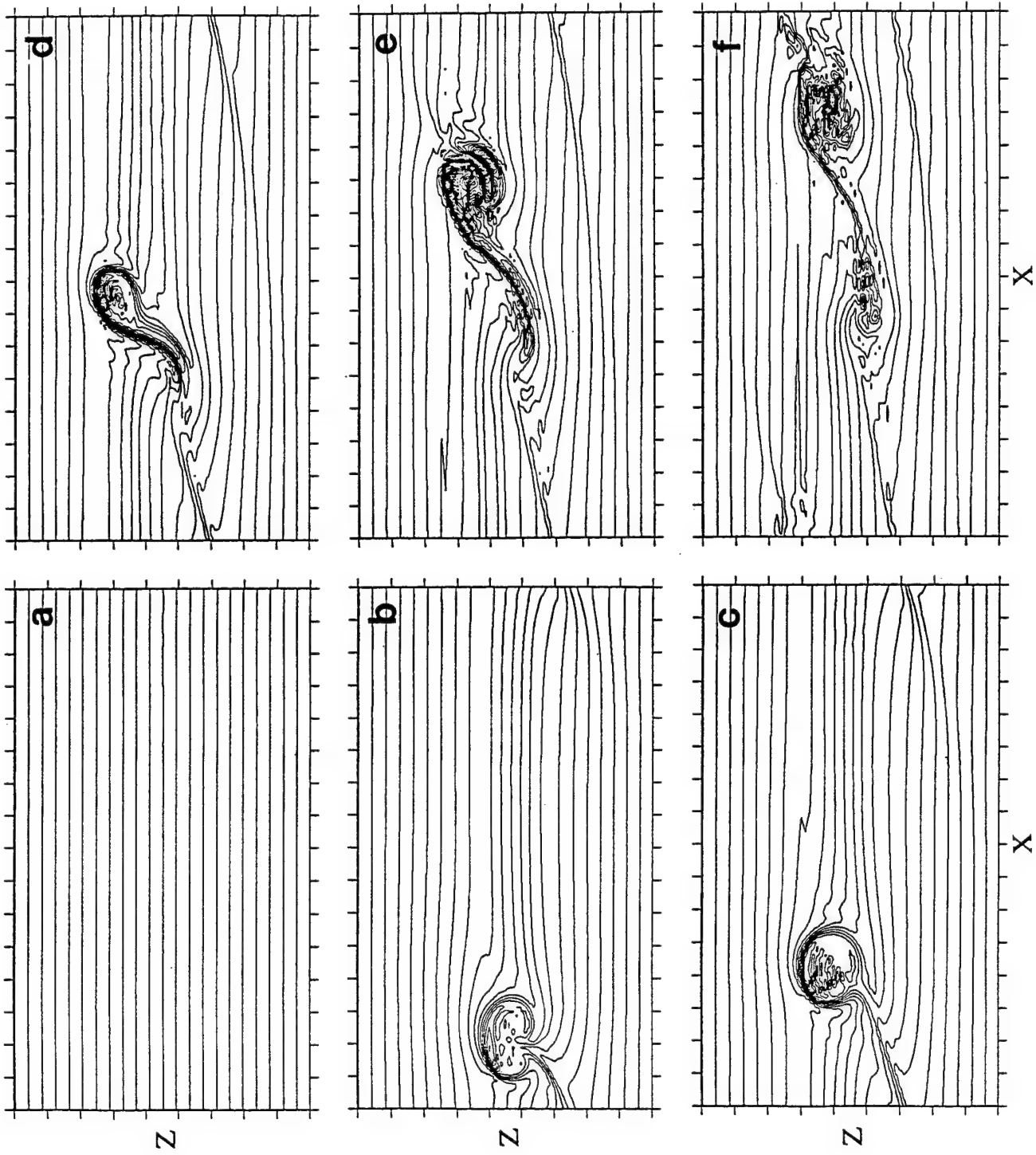
Figure 6.   As in Figure 2 for the case Ri = 0.5.

9
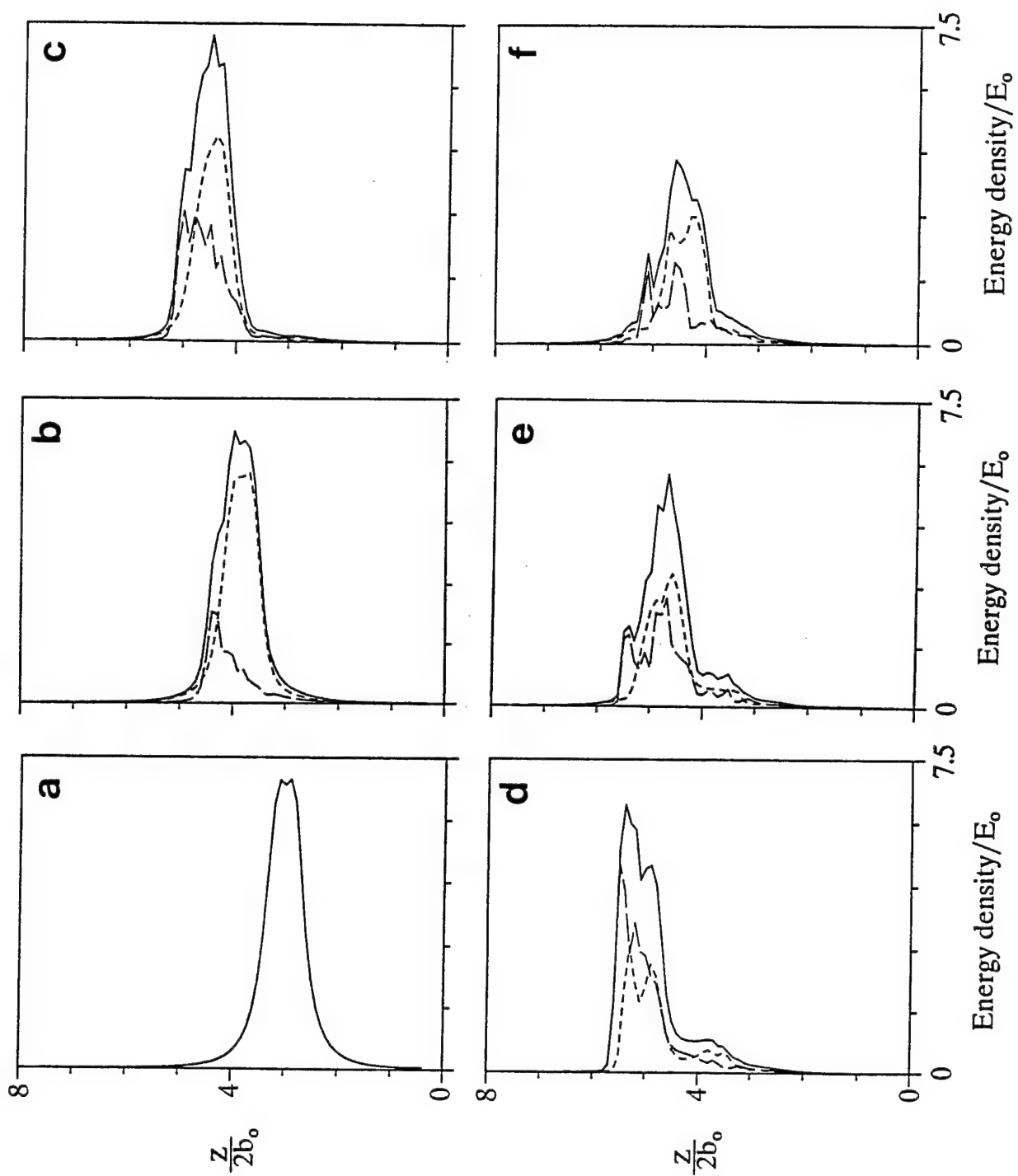
Figure 7.   As in Figure 3 for the case Ri = 0.5.

10
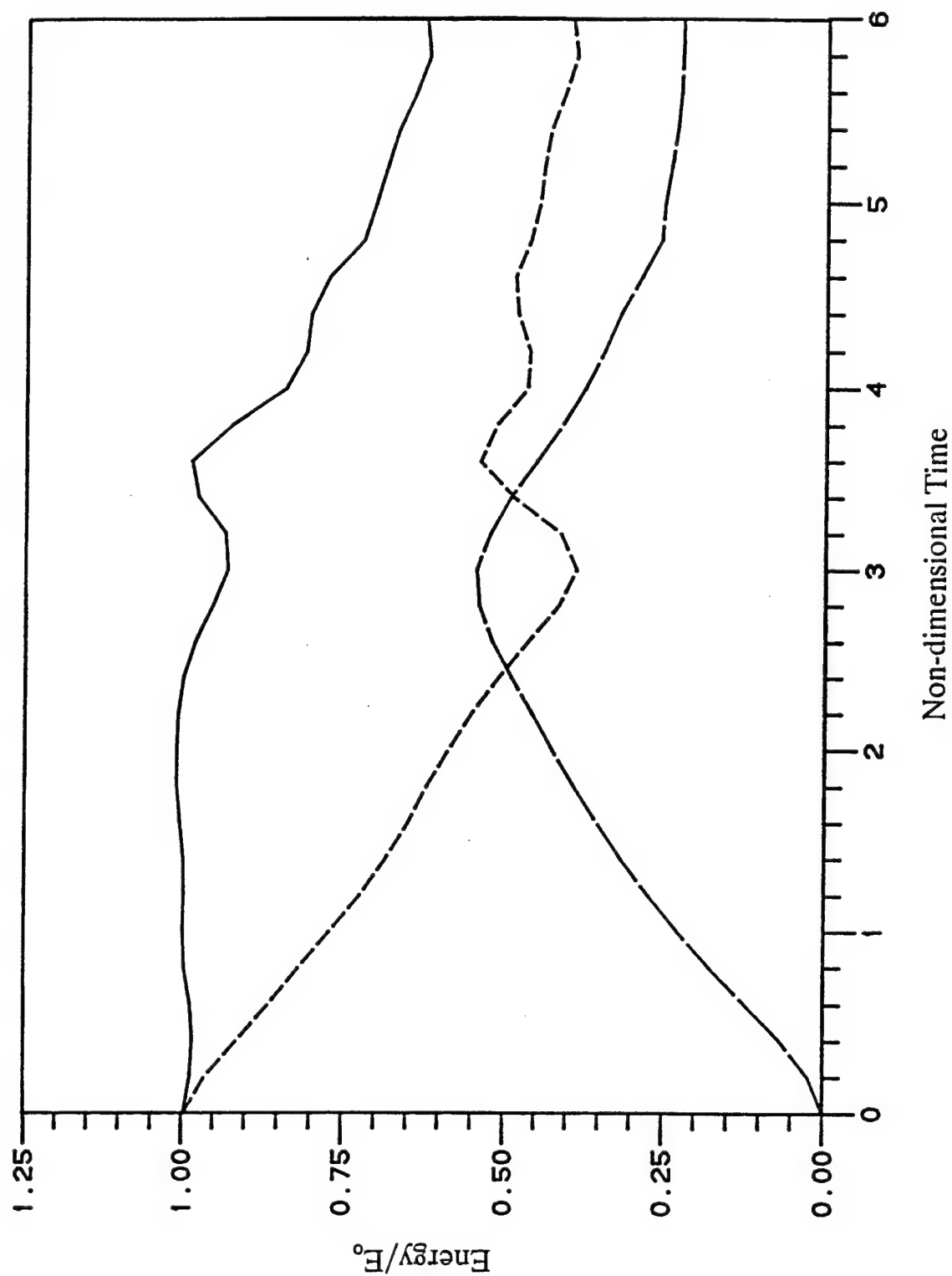
Figure 8.   As in Figure 4 for the case Ri = 0.5.

11

Figure 9 shows the effect of Richardson number on the evolution of a solitary vortex. This figure shows contour plots of perturbation vorticity for Ri = 0.5, 1, and 4 at a time of about 1 B-V period. With Ri = 0.5 or 1, a distinct, solitary vortex has developed, and the bulk of the clockwise vorticity is organized into a single vortex. This solitary vortex is significantly stronger than the countersign vorticity. In contrast, the Ri = 4 case shows that the maximum clockwise vorticity is about the same strength as the maximum counterclockwise vorticity. In this case, both vortices are decaying at about the same rate, and a solitary vortex has not formed.

Figure 10 is a summary plot of all the numerical calculations performed. The vertical axis in this figure represents flows with stratification and no shear, the horizontal axis represents flows with shear and no stratification, and the origin corresponds to flows with no stratification and no shear. In this figure, F_M is the ideal vortex migration number, F_S is a shear parameter analogous to F_M, N_o is the B-V frequency defined by eqn. (2), b_o is the initial separation distance between the vortex cores, and V_M is the ideal vortex migration speed. Straight lines through the origin are lines of constant Richardson number. The circles in Figure 10 are our numerical calculations, and the triangles and diamonds represent results of other investigators. Open symbols denote cases for which a solitary vortex evolved in the calculation; solid symbols represent cases for which a solitary vortex did not form.

Figure 10 shows asymmetric vortex evolution and the emergence of a solitary vortex whenever the Richardson number is of order one or less, and a symmetric evolution and decay when the Richardson number is greater than around one. When a solitary vortex emerges, it apparently is long-lived as the shear maintains the single vortical structure, thus increasing its lifetime. Note from above that typical oceanic Richardson numbers are around four or less, which is around the range found here for the emergence of solitary vortices. Thus, these results should be important in ocean applications.

4.2. Results From Delisi and Greene, 1990, *Journal of Aircraft, 27*, 968-971.

This study explored how far a vortex wake migrates in a nonstratified, nonsheared flow and how long it lasts before decaying to negligible levels. The major results of this study are shown in Figures 11 and 12. Figure 11 shows nondimensional height vs time measurements where

$$H = h/b_o \qquad\qquad (3)$$

and

$$T = V_o t/b_o \qquad\qquad (4)$$

where h is the vertical distance the vortices have migrated in time t, and V_o is the initial vortex migration velocity.
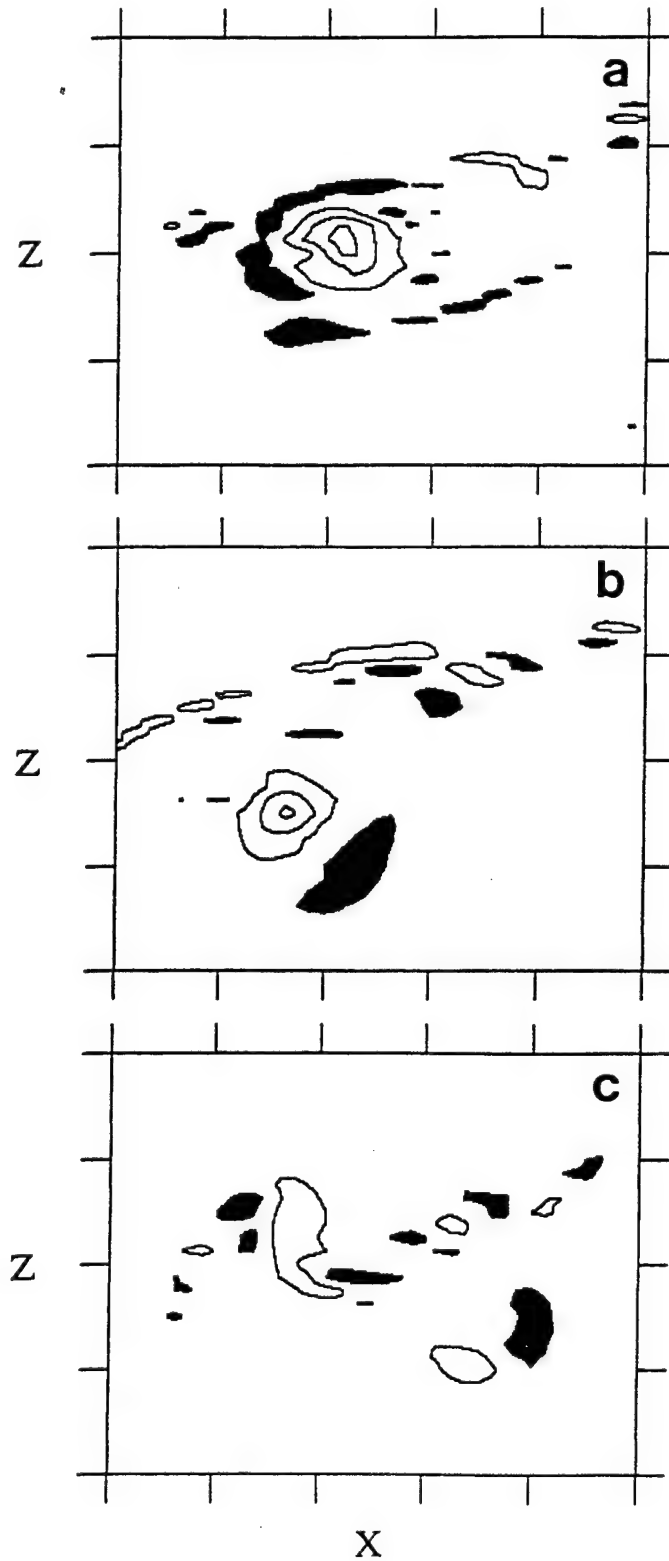
Figure 9.   Contours of perturbation vorticity at t = 6.   [White (black) shading signifies clockwise (counterclockwise) vorticity; (a) Ri = 0.5; (b) Ri = 1; (c) Ri = 4.]
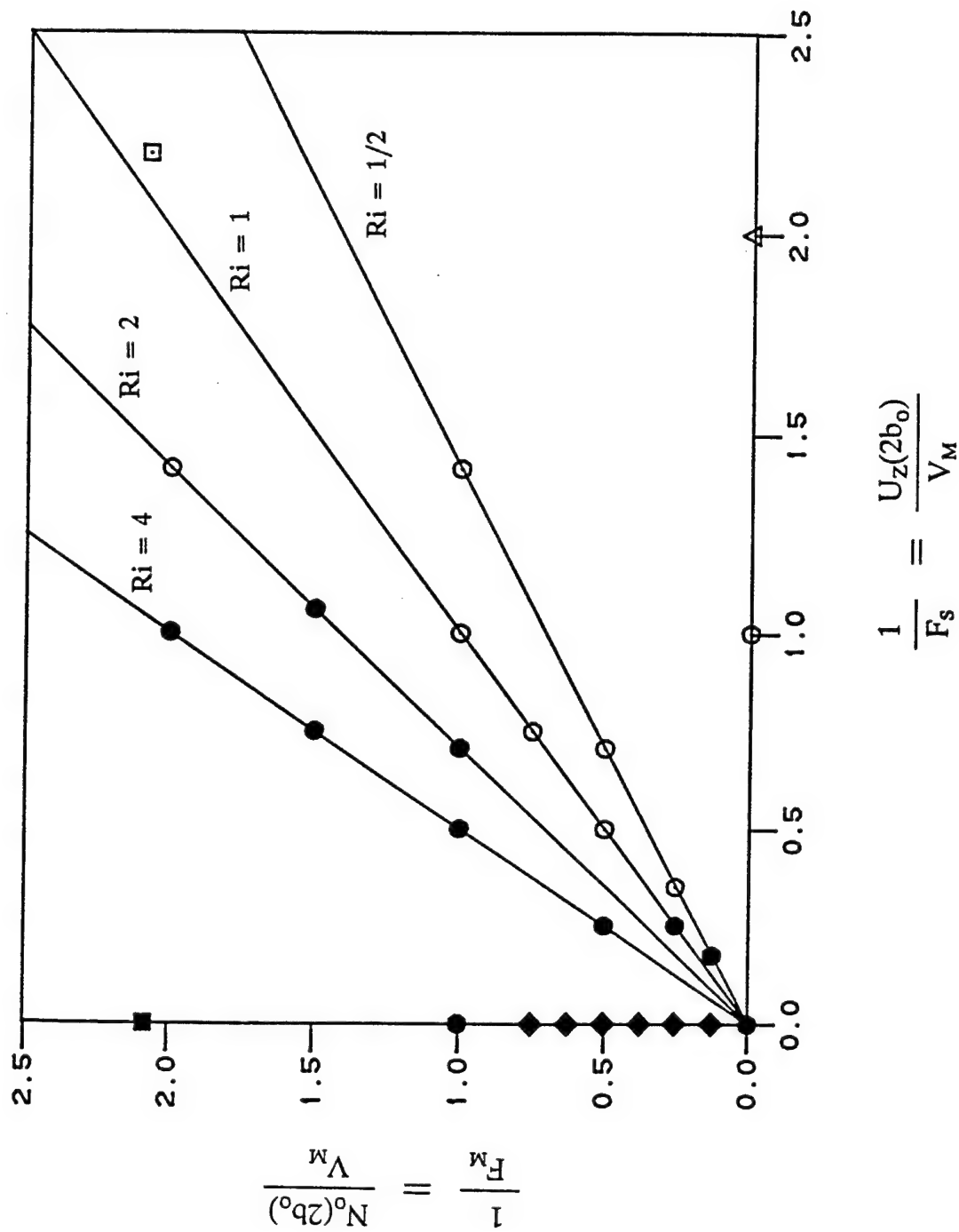
Figure 10. Summary data plot for the numerical simulations. Open (solid) symbols denote the occurrence (non-occurrence) of a solitary vortex at a time of one B-V period. The circles are our numerical results, the squares are for the numerical/experimental results of Delisi *et al* (1991), and the triangle represents the numerical calculation of Bilanin *et al* (1978). Diamonds and the closed circles on the vertical axis signify the experimental results of Barker and Crow (1977), Tomassian (1979), Sarpkaya and Johnson (1982), and Sarpkaya (1983). The horizontal and vertical axes represent reciprocals of the shear and stratification parameters; solid lines are constant Richardson number loci.

14
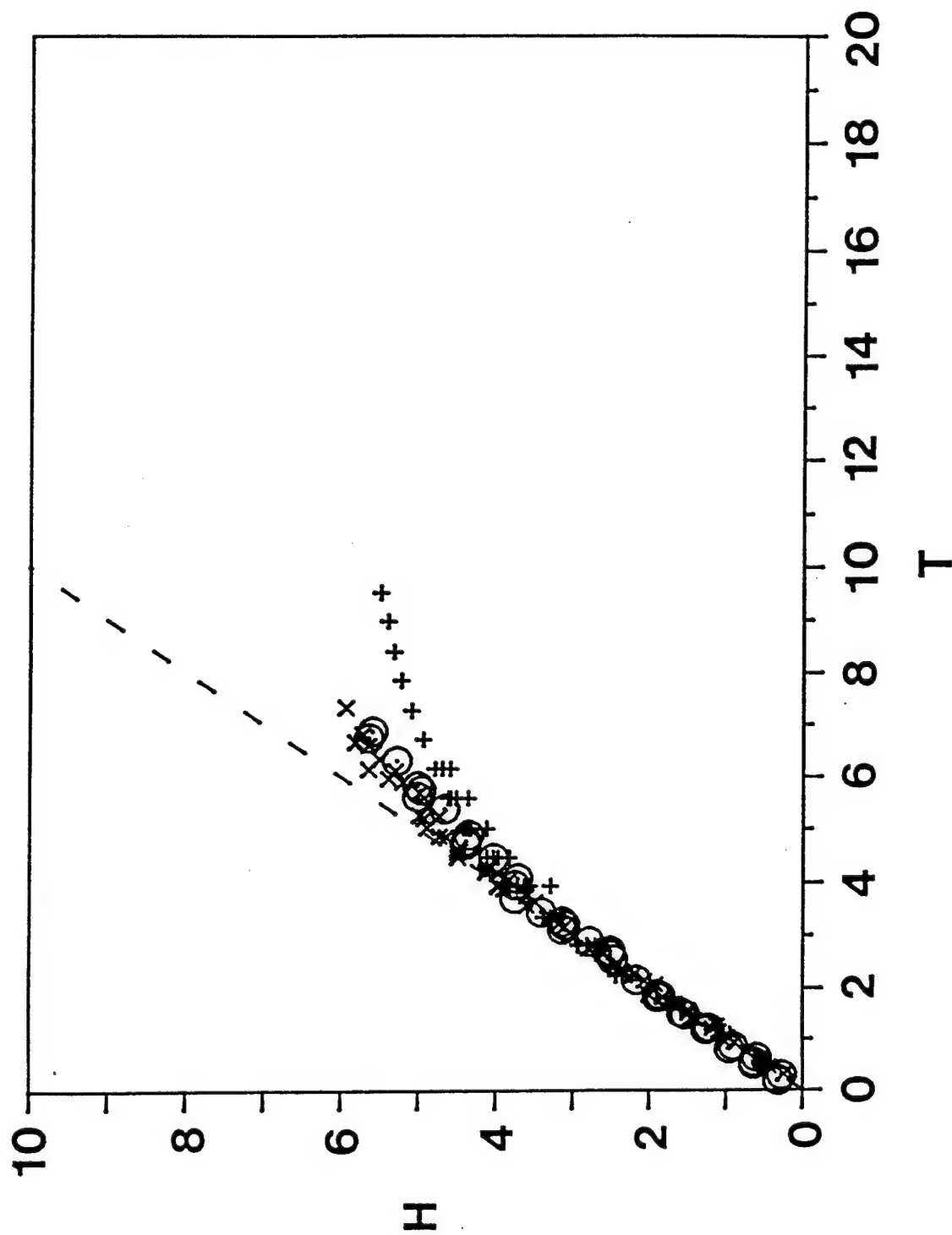
Figure 11. H versus T for laboratory vortex measurements in unstratified flows using dye for flow visualization. Xs are from Sarpkaya (1983), and plus symbols are from Tomassian (1979). The circles are our dyed-wake laboratory measurements. The dashed line is H = T.

15
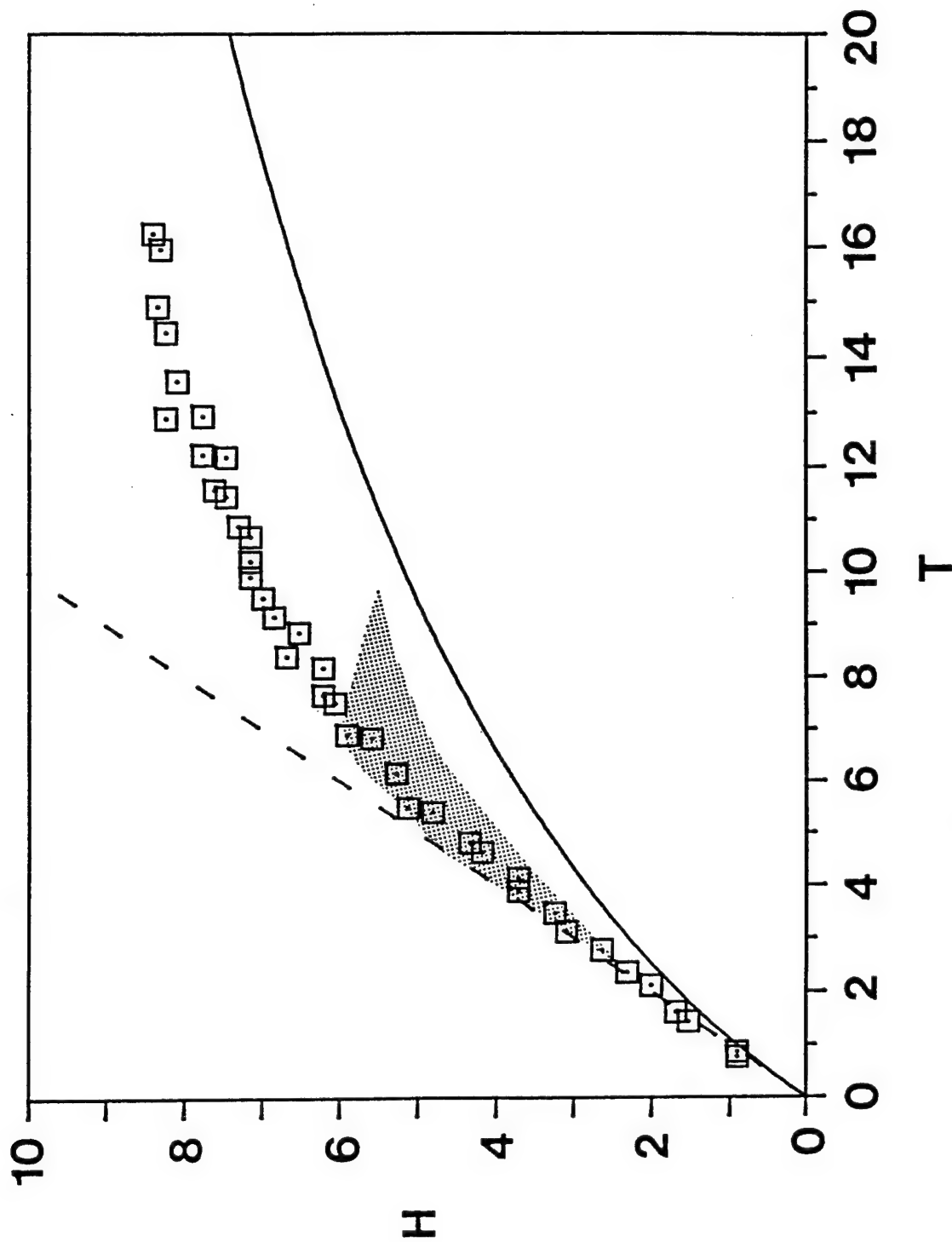
Figure 12.   H versus T for laboratory vortex measurements in unstratified flows.   Squares are our particle streak measurements. The stippled region encompasses the range of dye measurements from Figure 11.   The dashed line is H = T.   The solid line is a prediction from Greene (1986).

Figure 11 shows vortex measurements from a number of studies. The plus symbols in this figure are from Tomassian (1979), who generated two-dimensional vortex pairs with a plunger; the Xs are from Sarpkaya (1983), who generated a vortex pair with a three-dimensional wing; and the circles are from our measurements using a three-dimensional wing, similar to that of Sarpkaya. All measurements in Figure 11 used dye in the vortex cores to track the vortex migration. Thus, in all of these studies, dye was injected into the vortex cores, and the dye was followed with time as a means of tracking the vortex evolution. Figure 11 shows that all vortex migration measurements using dye for flow visualization are reasonably consistent, with the maximum migration distance, H_{max}, being around 6 and the maximum vortex lifetime, T_{max}, being around 9.

Figure 12 shows our measurements of H vs T when nearly neutrally buoyant particles were used to track the vortex motion. The stippled region in Figure 12 shows the range of dye measurements from Figure 11. Note that the particle measurements fall on top of the dye measurements for early times. This correlation indicates that both measurement techniques are consistent at early vortex times. The particle measurements, however, indicate an H_{max} around 8 and a T_{max} around 16, both of which are larger than the corresponding values in Figure 11. It is important to note in Figure 12 that the measurements were facility-limited in that the vortices hit the bottom of the tank before decaying. Thus, Figure 12 does not show either the maximum vortex migration distance or the maximum vortex lifetime.

There are important items to note from these results. Figure 12 shows that a vortex pair can migrate significantly farther and last significantly longer than previously thought. We now believe that the difference between our observations and those of previous investigators may be due to flow visualization differences (since dye, when diffused, may be difficult to observe) and/or to differences in the initial conditions of the vortices. Although this study was not able to measure either H_{max} or T_{max} because of the size of the facility, it did point out that both H_{max} and T_{max} may be significantly larger than indicated from previous studies. Additional results and comments on this topic are given in Section 4.4.

4.3.   Results From Delisi et al, 1991, *Physics of Fluids A, 3*, 2489-2491.

This study reported the first laboratory measurements of the evolution of a vortex pair in a stratified shear flow. The measurements were taken in a tilting tank measuring 488 cm long, 61 cm high, and 15 cm wide (Figure 13a; Thorpe, 1968, 1969, 1985). The tank was filled with linearly stratified salt water. To perform the experiment, the tank was filled and brought to the horizontal position. The tank was then tilted through a small angle, and the shear was generated (Figure 13b). At a prescribed time, the tank was again brought to the horizontal position, where the flow remained essentially constant. Vortices were generated by impulsively moving two wings which were initially at rest in the center of the tank. This wing motion resulted in two starting vortices, or a vortex pair. The evolution of this vortex pair was then followed until surges from the end walls disrupted the flowfield.

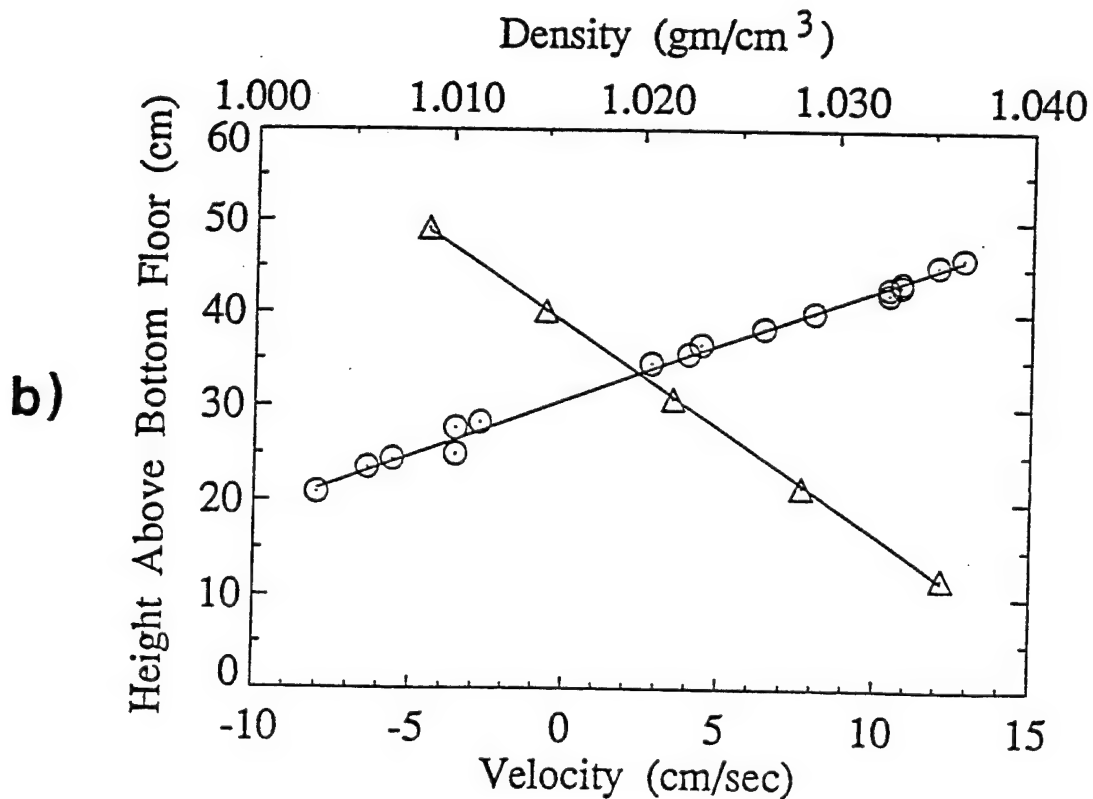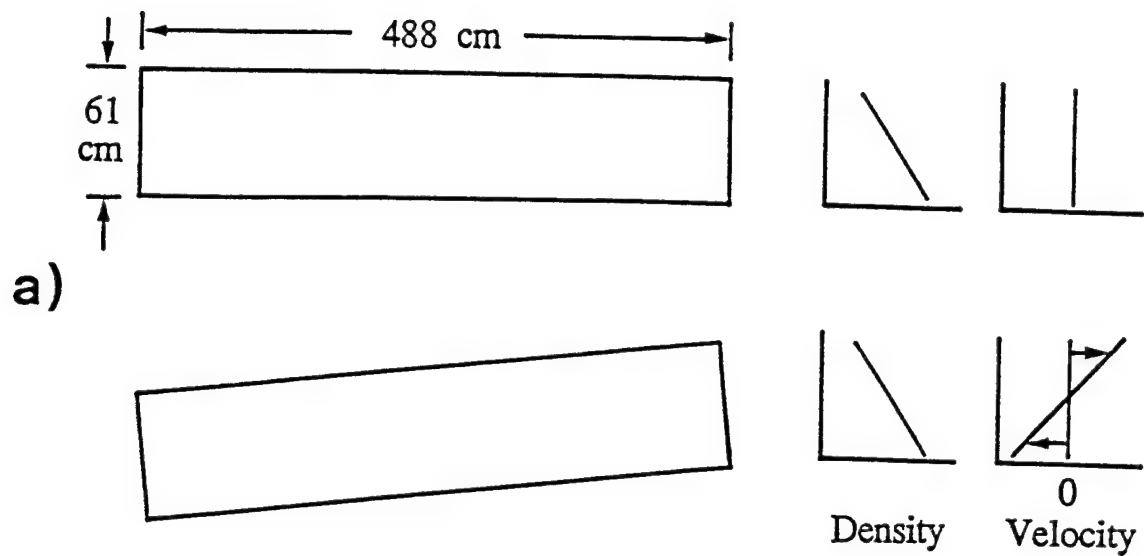Figure 13. (a) Schematic drawings of the tilt tank showing shear generation when the tank is tilted. (b) Measured density (triangles, upper axis) and velocity (circles, lower axis) profiles from the laboratory experiment. The solid lines are linear, least-square fits through the data. The deviations from a linear velocity profile occur where the wings disturb the flow, around a height of 27 cm above the floor.

18

Figure 14 shows results for a run with $N = 0.83$ sec^{-1} and $U_z = 0.84$ sec^{-1} (Ri = 1.0). In each figure, the top plot is a streak photograph from the laboratory experiment, the middle plot is total streamfunction from the numerical simulation, and the bottom plot is perturbation vorticity from the numerical simulation. The vorticity is contoured, with white (black) signifying clockwise (counterclockwise) vorticity. We nondimensionalize time by $\bar{t} = t/T_0$, where t is dimensional time and $T_0 = 2\pi b_0^2 / \Gamma_0$, where Γ_0 is the initial, unsheared circulation.

Figure 14 shows the flow at four times during the evolution. In Figure 14a, $\bar{t} = 0.10$. Both the laboratory and numerical plots show two stagnation points (one above, and another below, and to the left of the left vortex), and both show the same qualitative streamline shapes. The most important differences are in the shape of the vortices, which is due to the way the numerical vortices are modeled initially.

Figures 14b to 14d show succeeding stages in the evolution. All figures show similarities between the laboratory experiment and the numerical simulation. For example, both the laboratory and the numerics show the weakening and ultimate demise of the left vortex and the survival of the right vortex. This single vortex is what we call a "solitary" vortex. Note that the emergence of the solitary vortex occurs at approximately the same time in both the lab experiment and the numerical simulation.

Figure 15 shows the circulation versus nondimensional time for both the laboratory experiment and the numerical simulation. Because of the different sizes of each vortex, we estimated the circulation of each vortex over different radii, using a radius of 2 cm for the left vortex and 3 cm for the right vortex. The squares (diamonds) are estimates from the laboratory experiment for the left (right) vortex. The solid curves in Figure 15 are estimates for the same run from the numerical model. The agreement between the experiment and the model appears to be quite good for the left (rapidly decaying) vortex and reasonable for the right (surviving) vortex. Additional numerical results for this case are presented in Section 4.5.

4.4. Additional Laboratory Work

We have performed work extending the results of Delisi and Greene, 1990. In this work, we examined the evolution of the trailing wake vortex from just behind a wing to far downstream. Wing spans used in this study ranged from 3.8 cm to 9.9 cm. The laboratory facility proved too small even for the smallest of these wings under some conditions, as the wake vortices often reached the bottom floor of the tank. Smaller wings than those used were deemed not feasible due to the local effect caused by the small but finite strut holding the wing to the carriage.

19
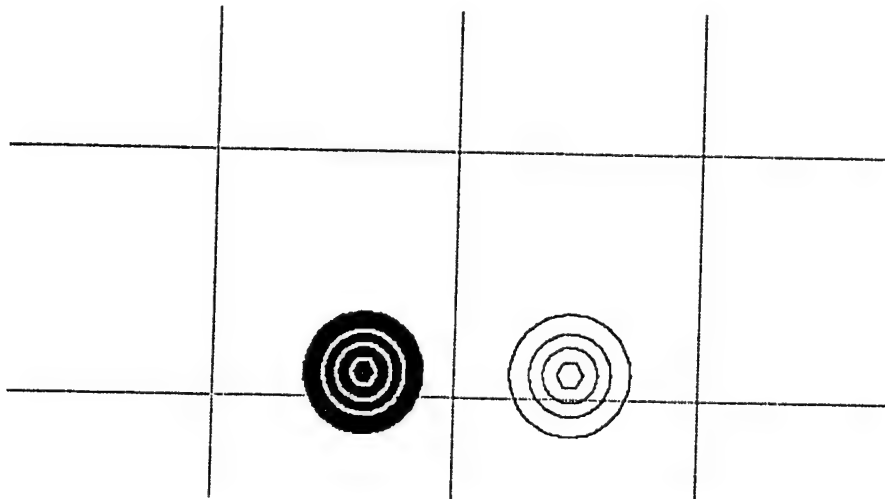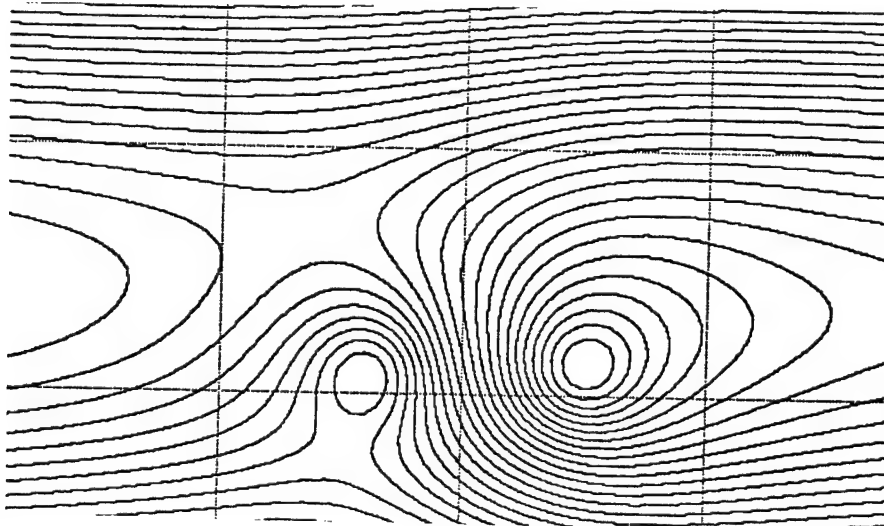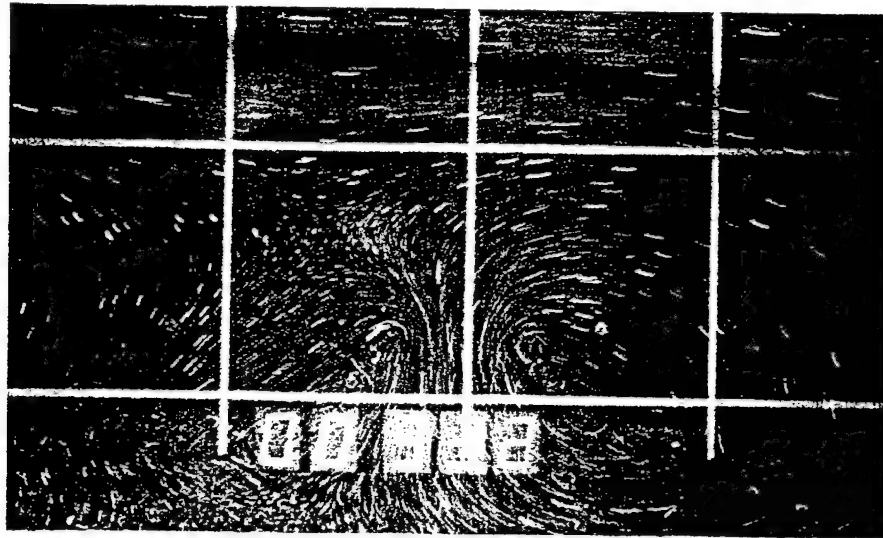
Figure 14. Vortex evolution in a stratified shear flow with Ri = 1.0. Laboratory streak photographs (top) and total streamfunction (middle) and perturbation vorticity (bottom) plots from a numerical simulation are shown for nondimensional times of (a) 0.10, (b) 0.36, (c) 0.62, and (d) 0.76. Horizontal and vertical grid separation is 10 cm.

20

Figure 14b.

21

Figure 14c.

22
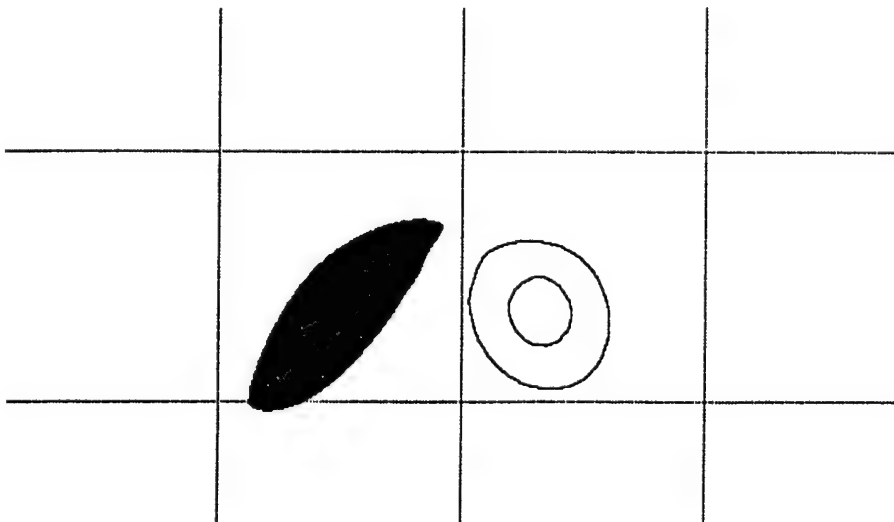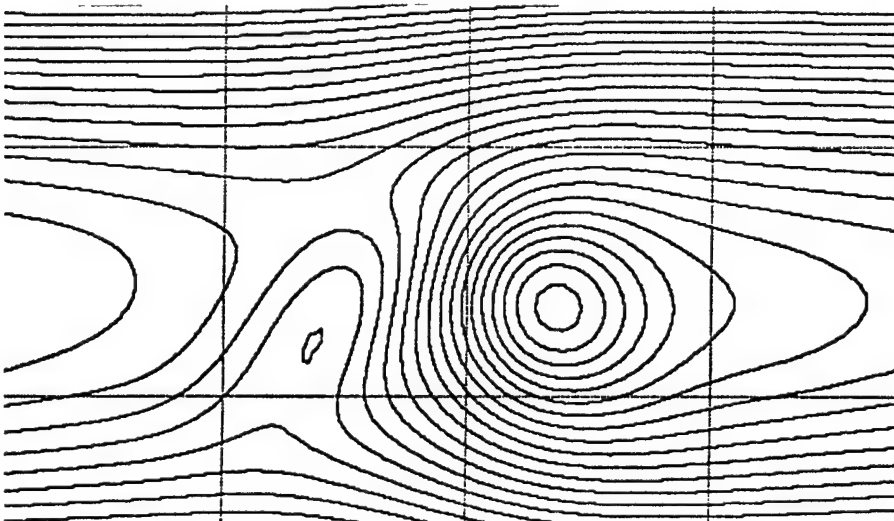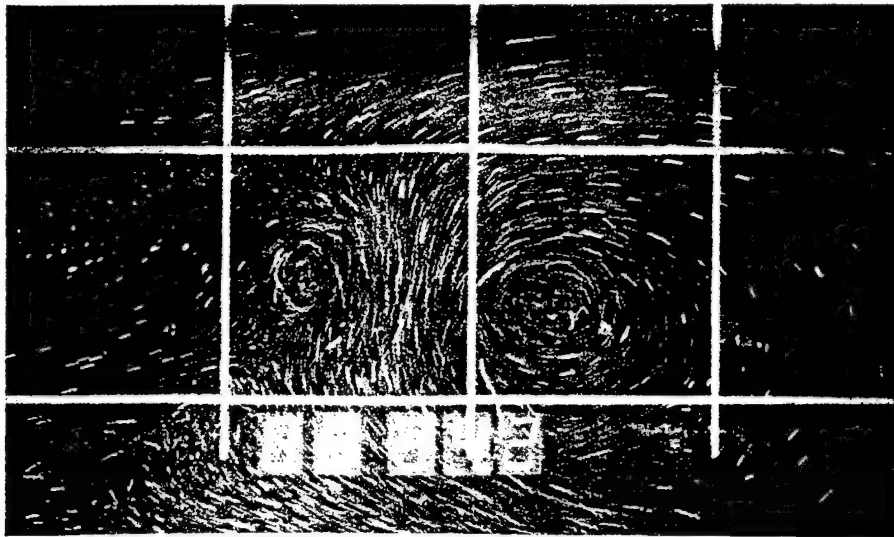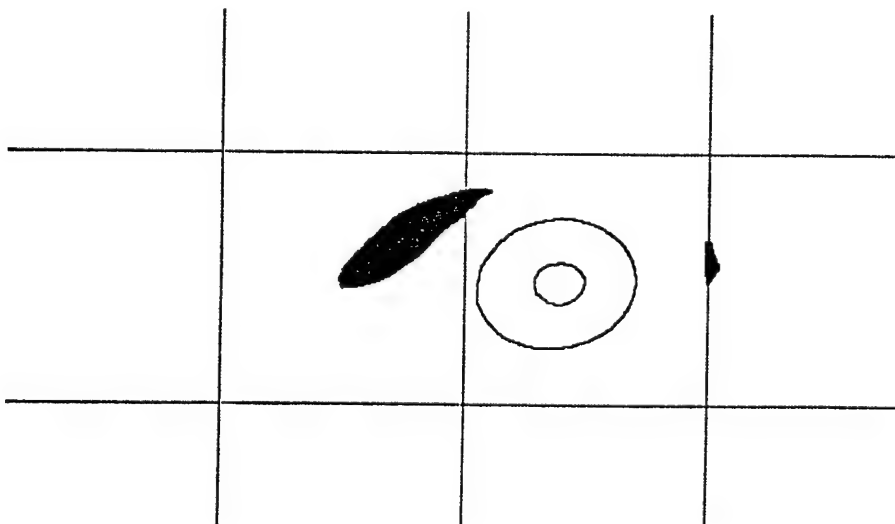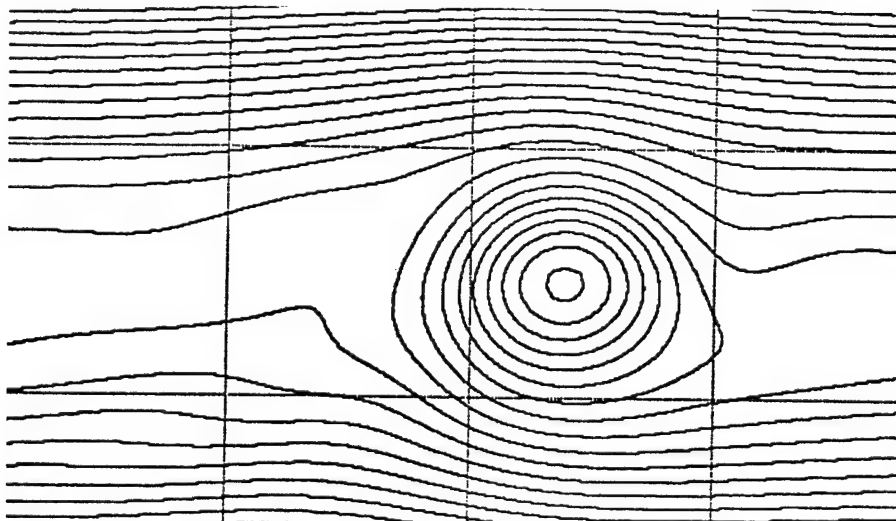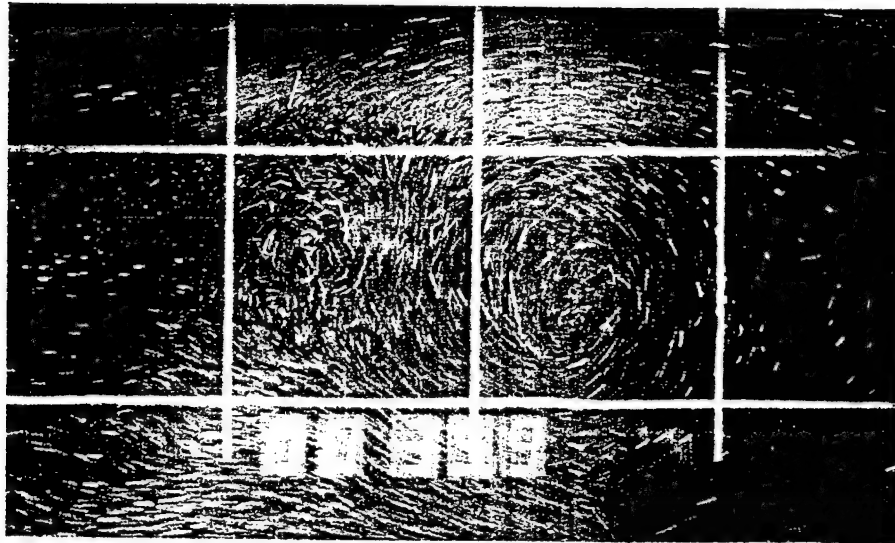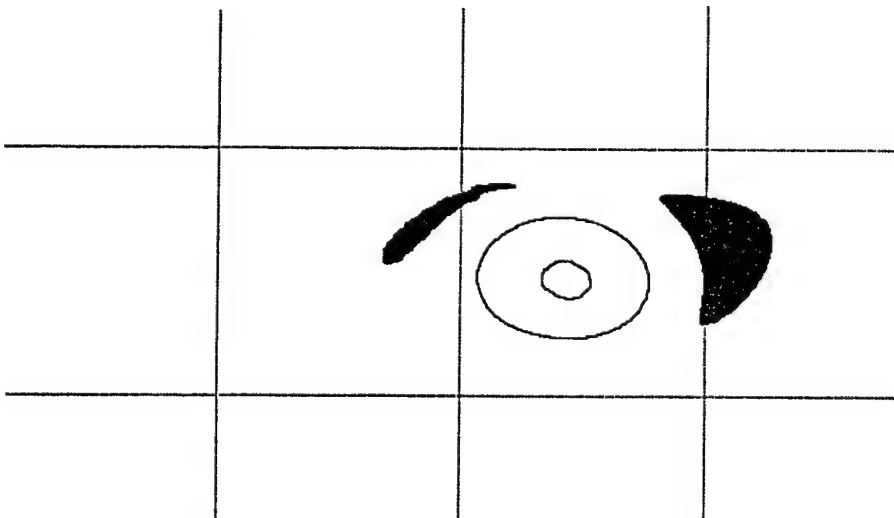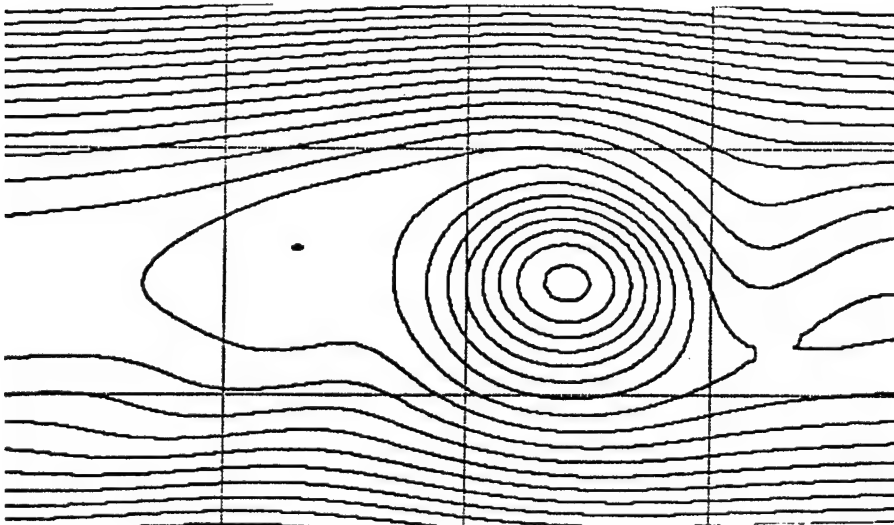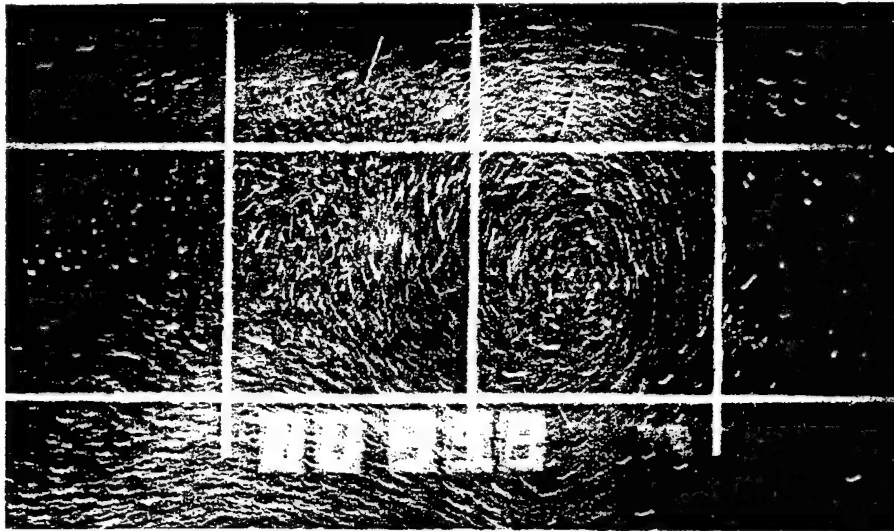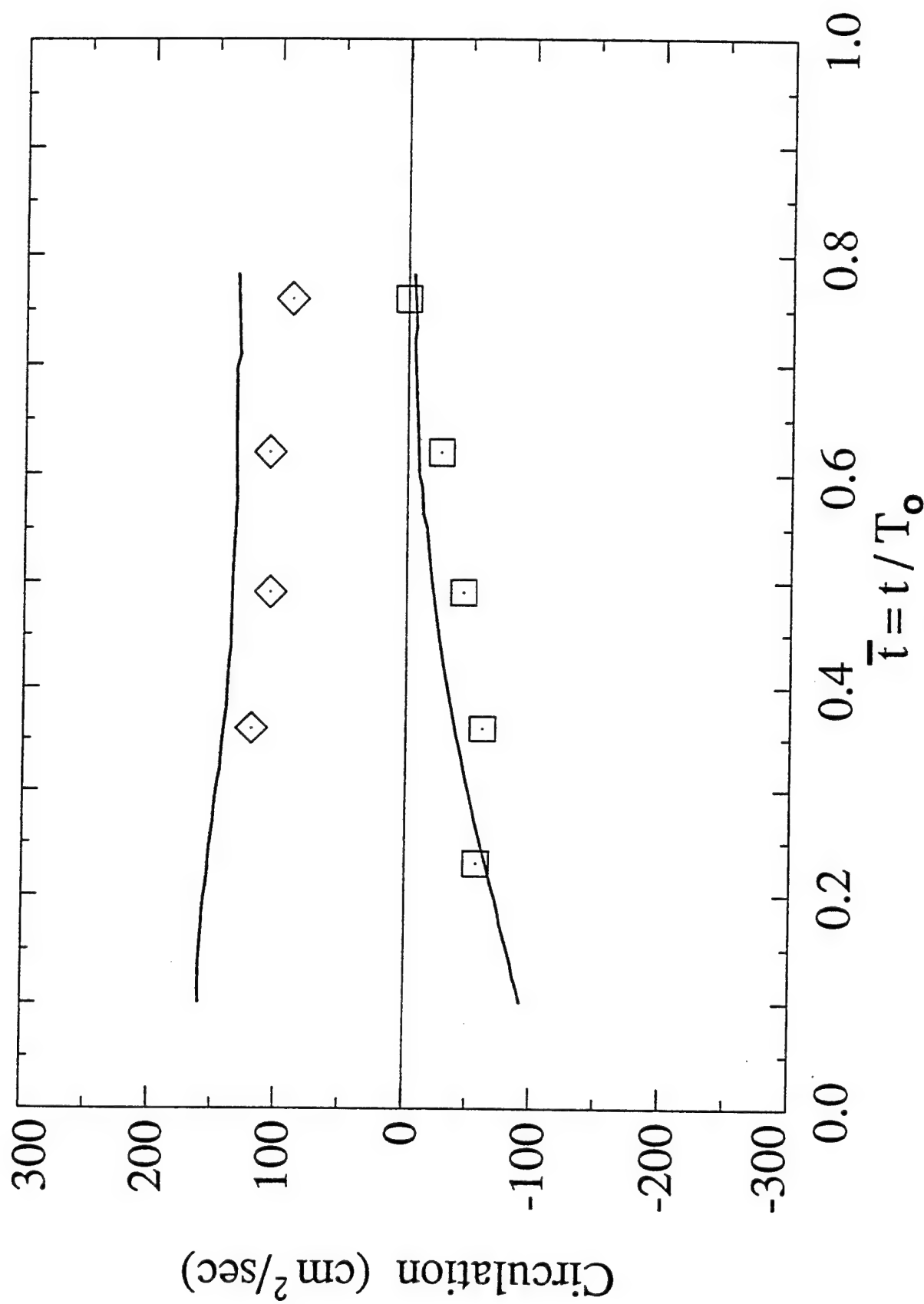
Figure 14d.

Figure 15. Circulation versus nondimensional time for the laboratory experiment and the numerical simulation for Ri = 1.0. The squares (diamonds) are measurements from the laboratory experiment for the left (right) vortex over a radius of 2 (3) cm. The solid curves are corresponding values from the numerical simulation.

Figure 16 shows streak photographs of the vortex flows as viewed from the side of the tank. The flow is illuminated with a vertical light sheet along the wake centerline. The wing has moved from left to right at the top of the tank, and the particles were introduced only in the very top of the tank, near the water surface. As the vortices propagate vertically downwards into the tank, some of the particles are entrained by the vortices, making the flow visible. In each succeeding photograph, the wake moves farther into the tank, away from the surface.

In Figure 16a, the trailing wake is a two-dimensional (2-D) line vortex pair at the bottom edge of the region with particles. In Figure 16b, the wake is beginning to show some nonuniformity in the axial direction. In Figure 16c, the wake is becoming distinctly three-dimensional (3-D). In Figure 16d, three vortex rings have evolved from the 2-D line vortex pair. The rings are being cut down the center by the light sheet, with half the ring on each side of the light sheet. The remaining photographs, Figures 16e to 16h, show the vertical migration of these 3-D rings, essentially unchanged, to the bottom of the tank.

Figure 17 shows schematic drawings of the flow fields in Figure 16 at two times in the evolution. For each of the two times, there is a 3-D view and a side view (the latter corresponding to the photographs in Figure 16). In Figures 17a and 17b, the vortices are 2-D line vortex pairs, corresponding to the photograph in Figure 16a. In Figures 17c and 17d, the flow has evolved into 3-D vortex rings, corresponding to the flow in Figures 16d to 16h.

The 2-D to 3-D evolution shown in Figures 16 and 17 is the mutual induction, or Crow, instability (Scorer, 1958; Crow, 1970). Crow predicted that the most unstable wavelength was 8.6 b_0. His theory was developed for nonstratified, nonturbulent, nonsheared flow. Although Crow instability has been observed before, the resulting vortex rings decayed rapidly in previous observations (e.g., Sarpkaya, 1983). This is the first study in which the 3-D rings are long-lived.

A different view of the vortex evolution is shown in Figure 18. Here, we show photographs of the bottom floor of the tank after the vortex motion has disturbed an initially uniform distribution of particles on the tank floor. In Figure 18a, the wing was at a height of 2.5 spans above the floor, and the edges of the disturbance are nearly straight, parallel to the side walls of the tank. This pattern indicates that the disturbance is nearly 2-D. In Figure 18b, the wing was at a height of 5 spans above the floor. Now, the edges of the disturbance on the floor are wavy, indicating the onset of Crow instability. In Figure 18C, the wing was at a height of 8 spans above the floor. At this height, the disturbances on the floor are three-dimensional.

Figure 19 shows our measurements using particles to track vortex flows like those shown in Figure 16. In this figure, the floor is at H = 26, and many of the vortices eventually strike the floor. Measurements are only shown to H = 22, however, because of difficulty in seeing near the floor and due to ground effects when the vortices approach a solid surface.
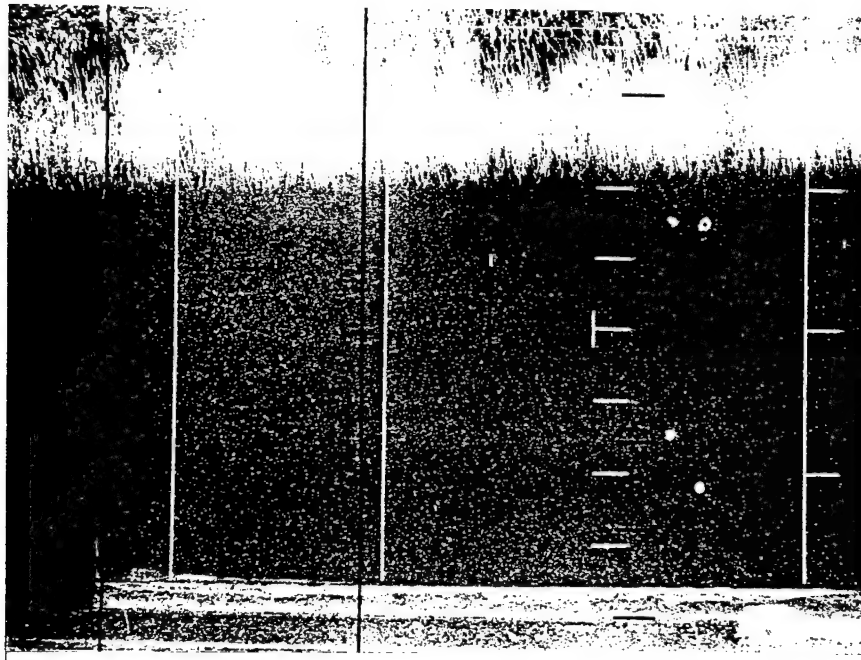
Figure 16a
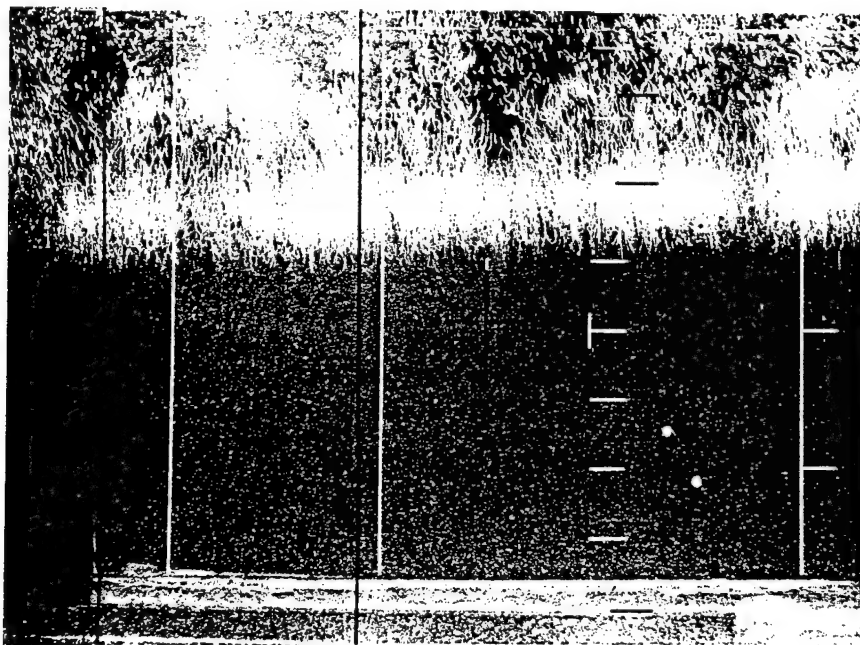
Figure 16b

Figure 16. Vortex evolution from a wing in an unstratified flow. Streak photographs are shown for the 5.1 cm span wing at an angle of 13 deg and a towing speed of 324 cm/sec. Values of T are: (a) 2.8, (b) 5.3, (c) 7.8, (d) 10.3, (e) 12.8, (f) 15.3, (g) 17.8, and (h) 20.2.
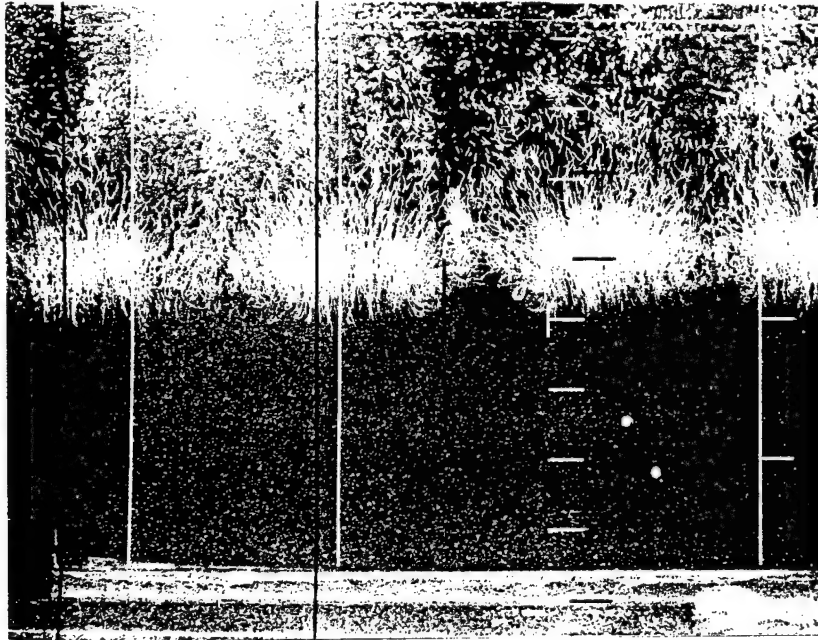
Figure 16c

Figure 16d

27
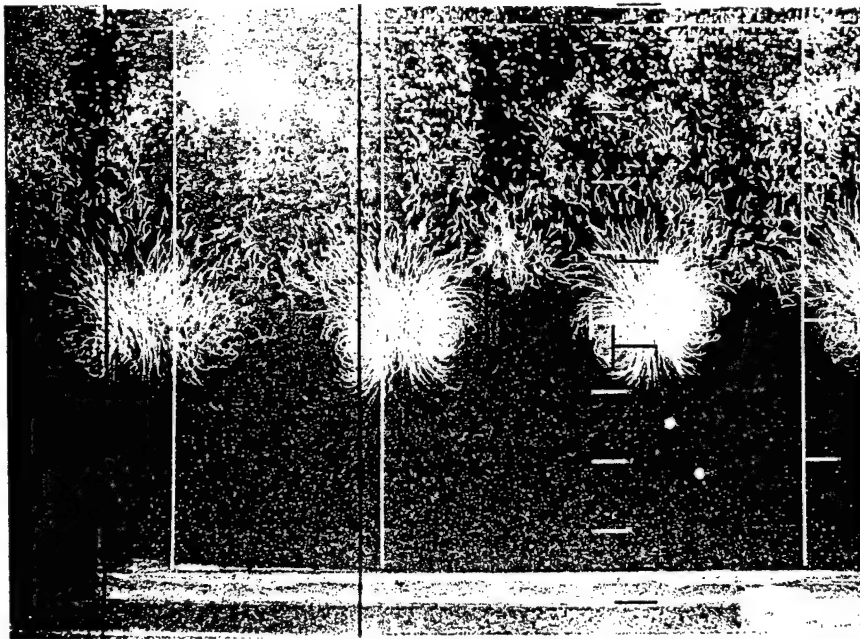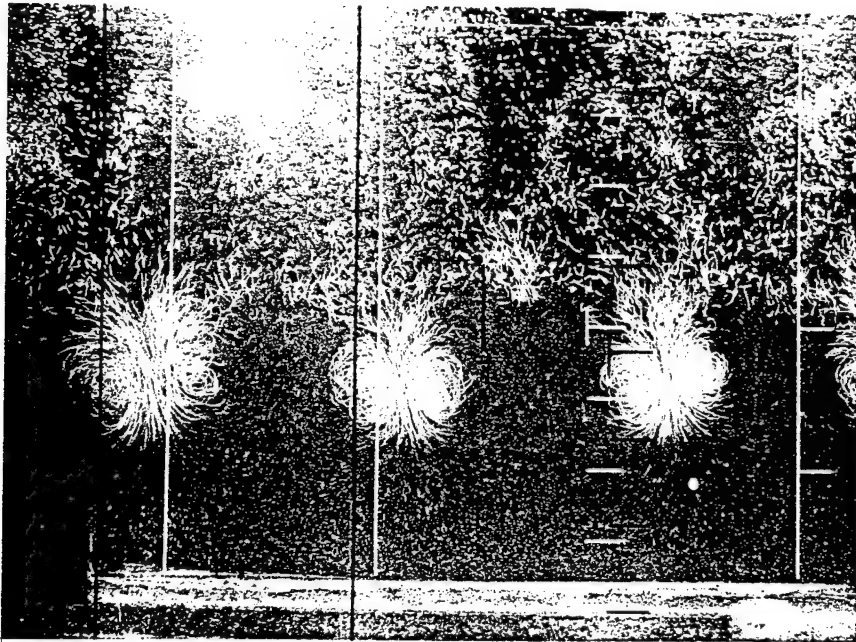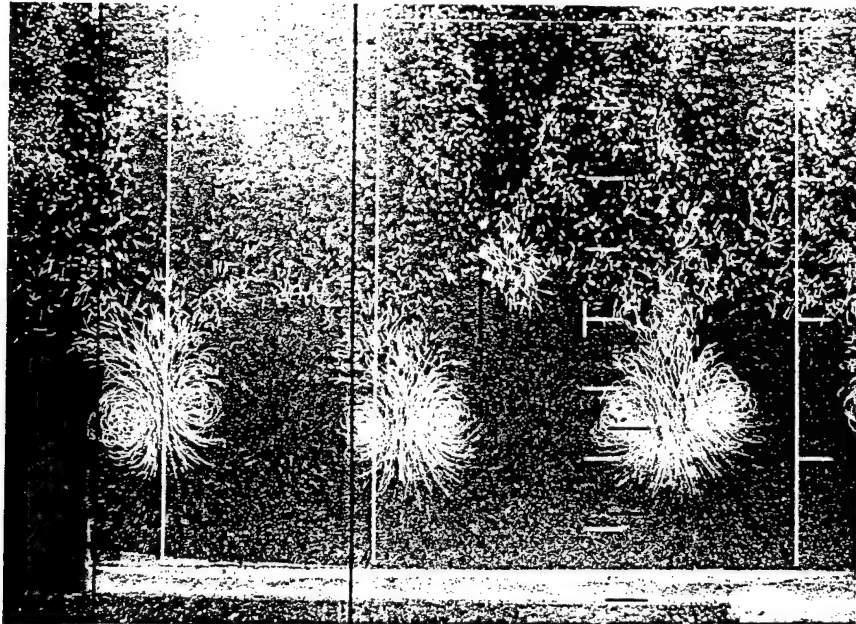
Figure 16e

Figure 16f

Figure 16g

Figure 16h

29
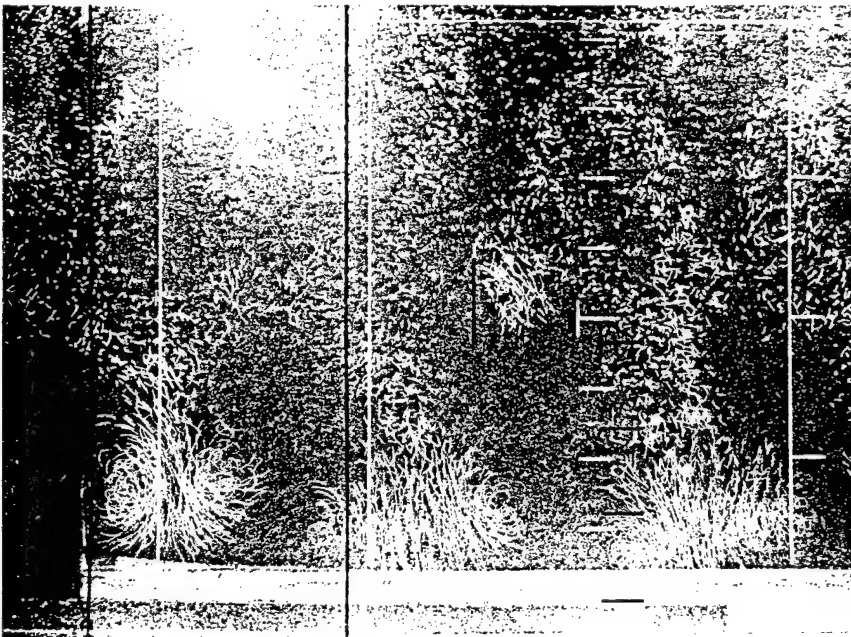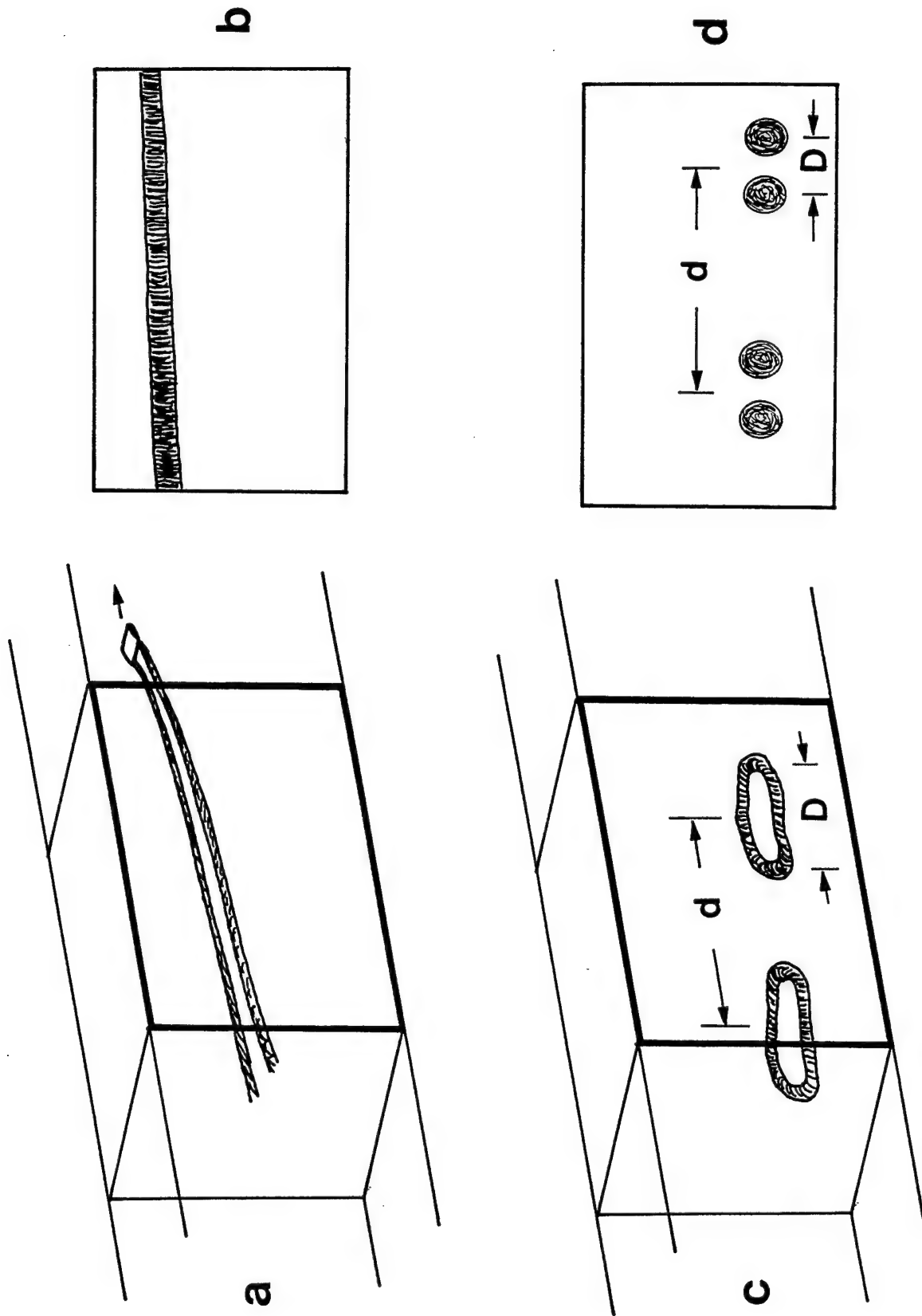
Figure 17. Drawings of the flow field shown in Figure 16 at two times in the evolution of a vortex wake. Figures 17a and 17b show the three-dimensional and side view, respectively, of the flow field at an early time, while the wake is two dimensional. Figures 17c and 17d show the corresponding views at a later time, after the wake has evolved into three-dimensional vortex rings.
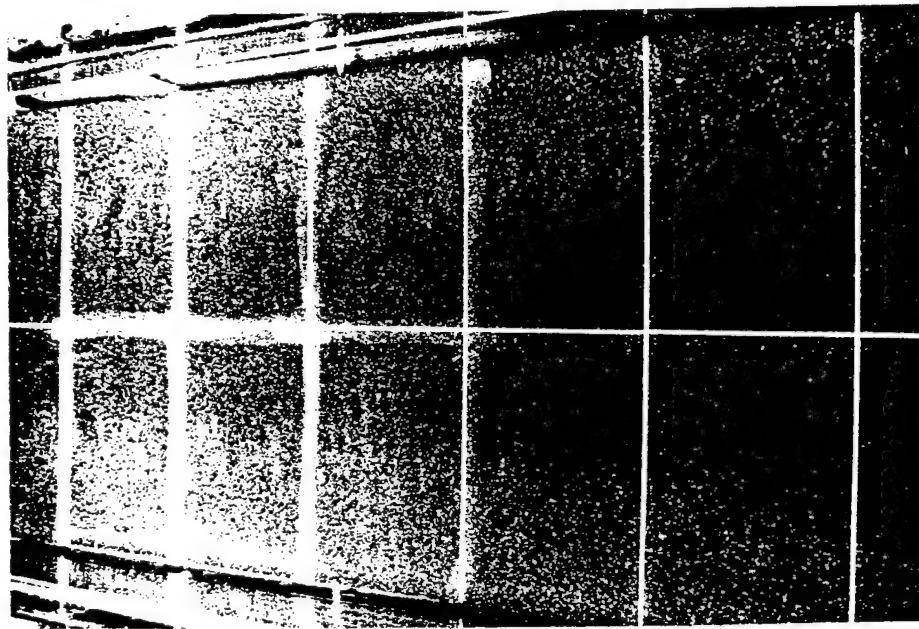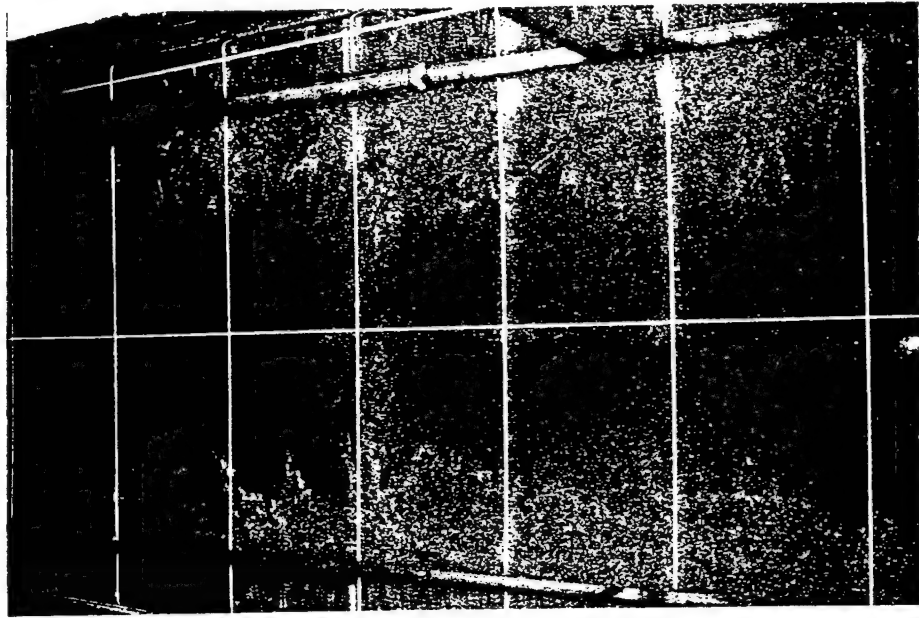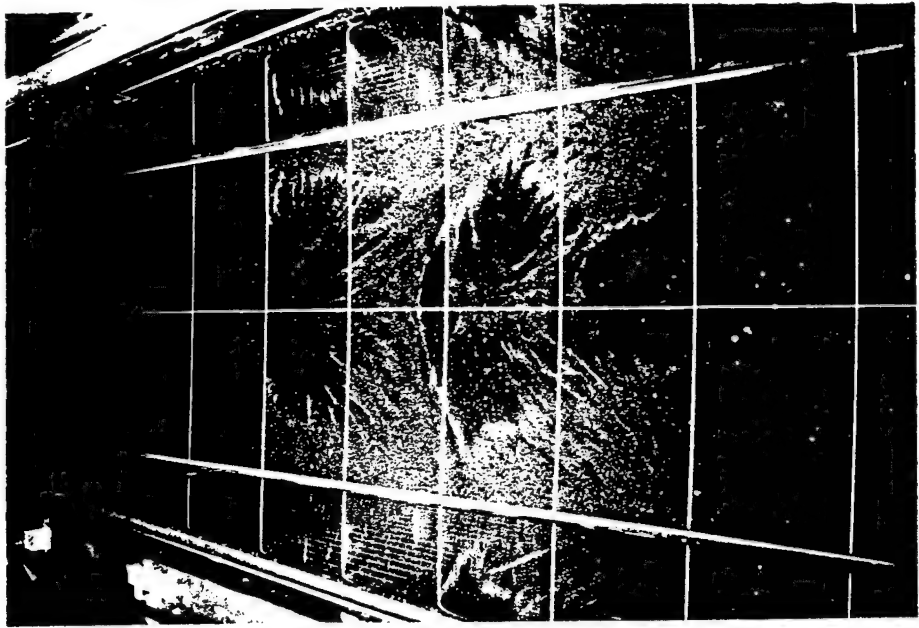
Figure 18. Photographs of the bottom floor with an initially uniform distribution of particles. Data are for the 9.9 cm span wing at a towing speed of 200 cm/sec. The distance of the wing above the floor was (a) 2.5 spans, (b) 5 spans, and (c) 8 spans.

a   b   c

31
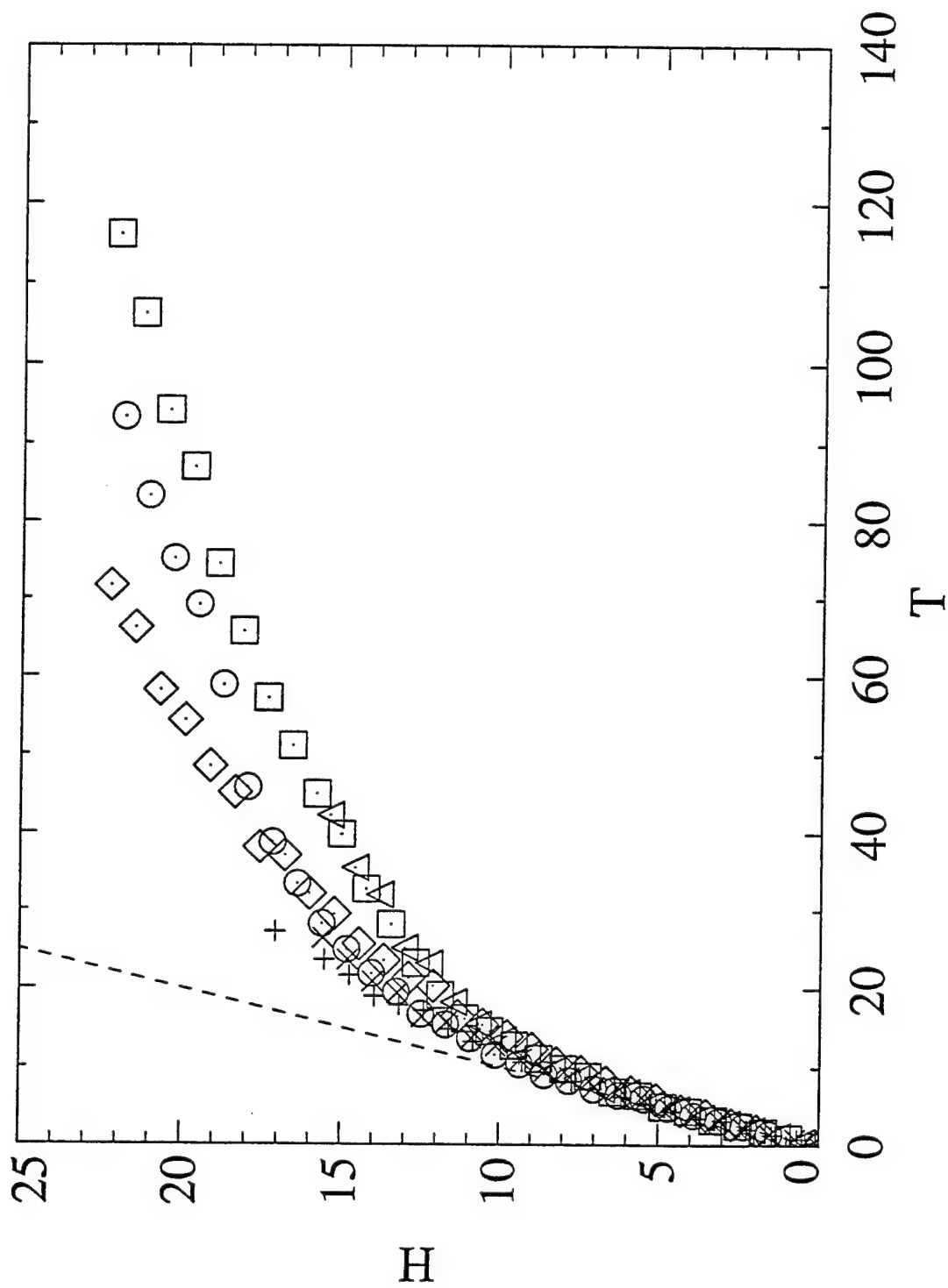
Figure 19.   H *vs* T for the 3.8 cm span wing using particle streak measurements at a towing speed of 324 cm/sec.   Each run is marked with a different symbol.   The bottom floor is at H ≈ 26.

The differences between Figure 19 and the earlier vortex evolution using dye and a tracer (cf. Figure 11) are the following. First, dye can diffuse and can be difficult to observe. In our experiments, dye in the vortex cores often diffused rapidly when the vortex motion transitioned from 2-D to 3-D. If insufficient dye is used to mark the vortex motion, the dye can diffuse, giving the misleading impression that the vortices have decayed.

Second, our recent vortex measurements indicate that H_{max} is a function both of the lift and drag on the airfoil and on the Reynolds number. These parameters appear to affect the vortex reconnection in the transition from 2-D line vortices to 3-D ring vortices. If the lift or Reynolds numbers are low or the drag is high, the reconnection is weak, and energetic rings are not formed. In this case, H_{max} can be as low as around 6. If the lift is large and the drag is low, the reconnection is strong, and energetic rings are formed. In this case, H_{max} can be 20 or greater. Additional studies are currently being performed to quantify these effects. However, it appears certain at this point that stronger initial vortices will propagate farther than weaker initial vortices. Thus, the thought that weaker vortices will propagate as far as stronger vortices but will merely take longer may be untrue.

Additional laboratory measurements were also performed on the evolution of a vortex pair in a stratified, shear flow. These measurements are described briefly below.

These measurements were made in the tilting tank described in Delisi et al (1991) and shown in Figure 13. In this additional study, the Brunt-Vaisala frequency was zero (nonstratified), 0.33, and 0.2 sec^{-1}. The bulk of the runs were performed with $N = 0.328 \pm 0.007$ sec^{-1} (average over 12 runs). For all runs, the motion of the wings (and, hence, the initial vortex strength and spacing) was kept constant.

The rise of the vortices in a nonstratified, nonsheared flow is shown in Figure 20. This figure shows depth versus time of the left and the right vortex for five nominally identical runs. The average of the five runs is shown in Figure 21. Note that the left vortex rises slightly higher than the right vortex, indicating a slightly stronger right vortex. We believe this asymmetry in vortex strengths is due to an asymmetry in the motion of the two wings which generate the vortices.

The vortices are formed behind each wing and in the wake of the strut holding each wing. The effect of the struts appears to be a somewhat erratic motion of the vortices in the first half-second of evolution. Because of this, the first half-second of motion is excluded in the plots.

From Figure 21, the average velocity of initial vertical migration of the left vortex is 5.0 cm/sec, and the average velocity of the right vortex is 4.6 cm/sec. The average of the two velocities is 4.8 cm/sec. During this time, the average separation distance between the vortices is 13.4 cm.

Figure 20. Depth vs time for vortices from five nominally identical runs in the tilt tank in a nonstratified, nonsheared flow.
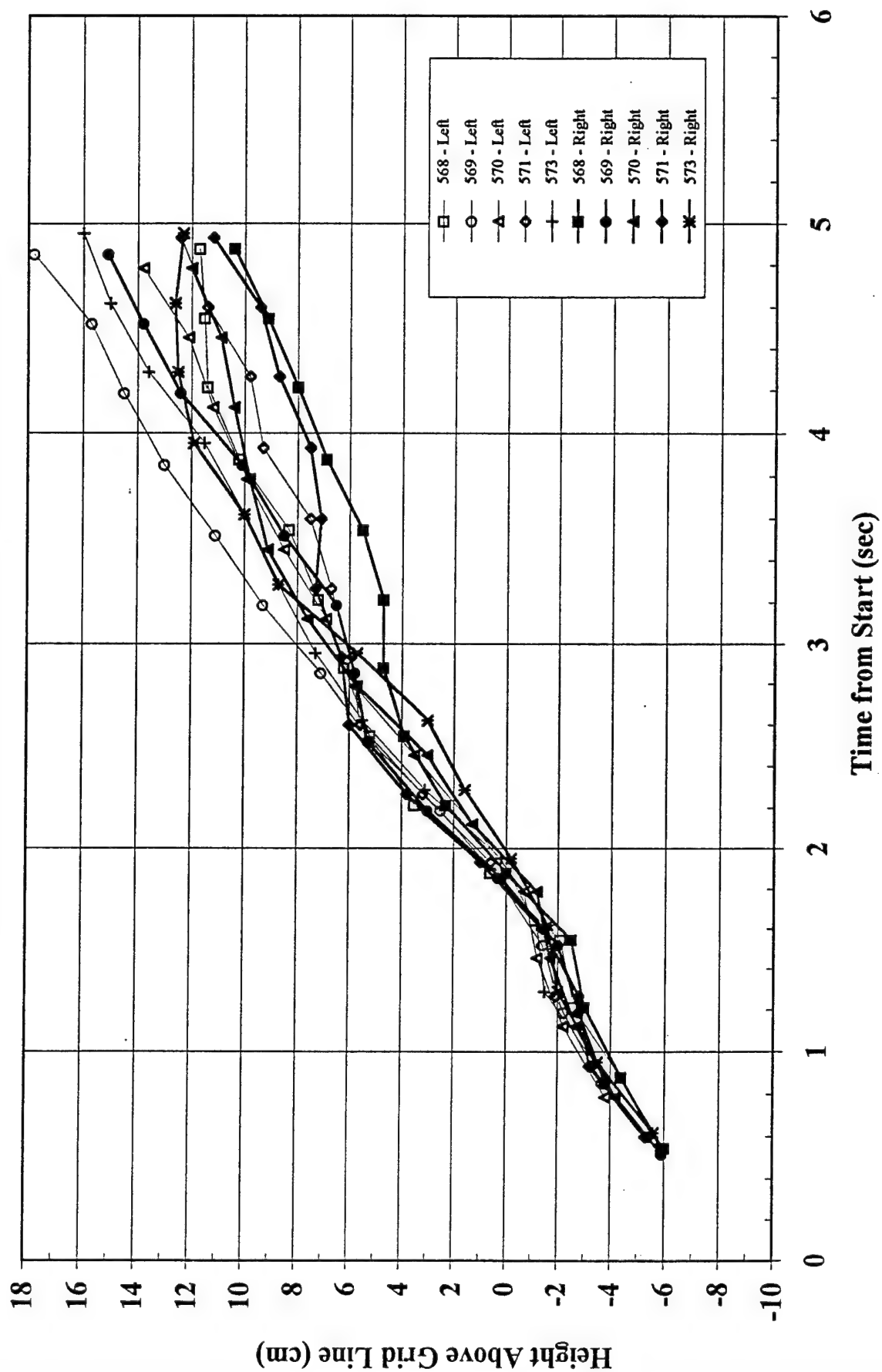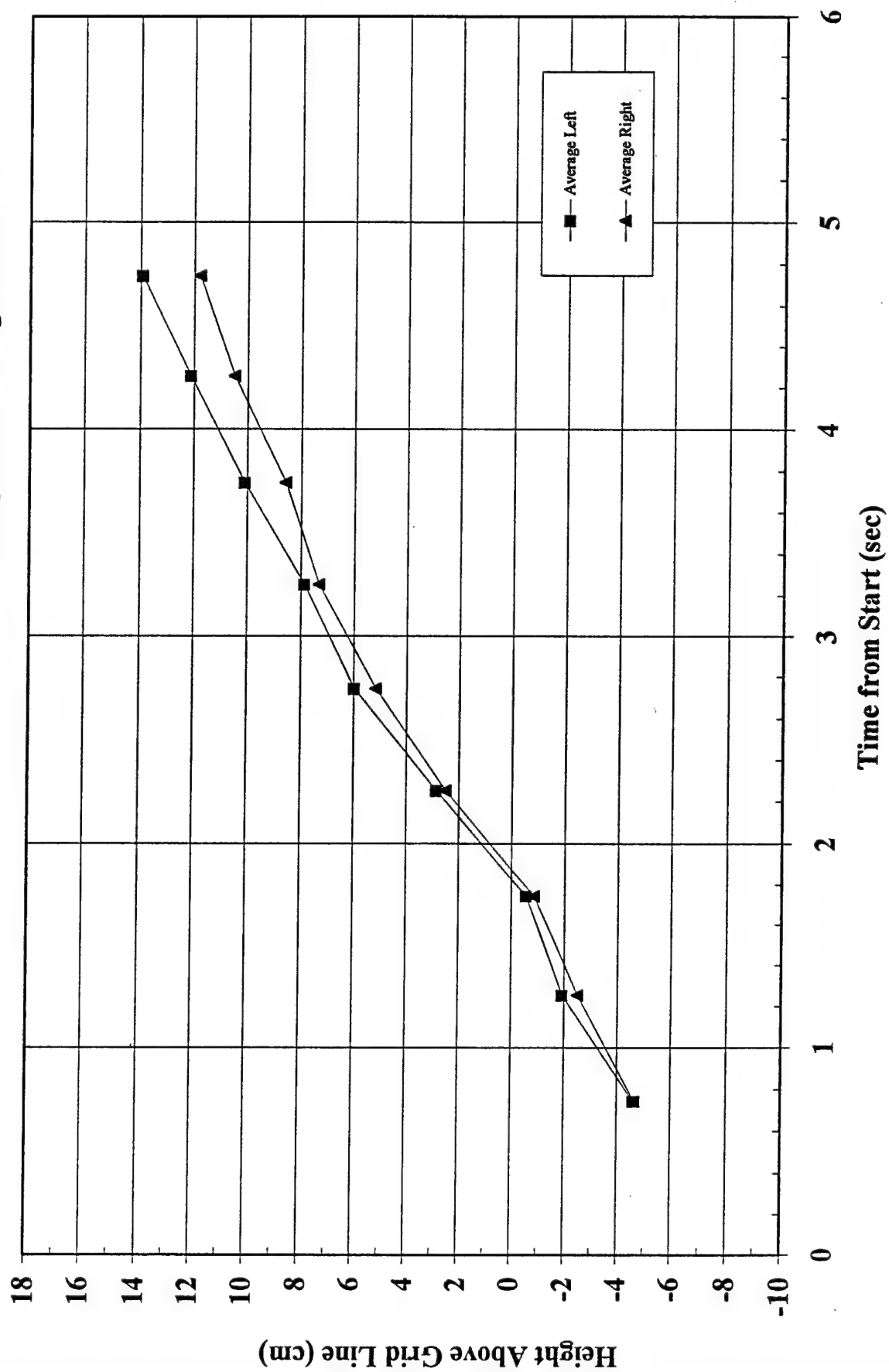
Figure 21. The average of the data shown in Figure 20.

35

When stratification is added to the flow, the vertical migration of the vortices is suppressed (Tomassian, 1977; Sarpkaya, 1983; Liu and Srnsky, 1990). The vertical migration of the vortices in our study in an unsheared flow with $N = 0.33$ sec^{-1} for five nominally identical runs is shown in Figure 22. The average of the data in Figure 22 is shown in Figure 23. Note that, relative to Figure 21, the data in Figure 23 show a reduced vertical migration, as expected.

Using an initial vertical velocity of 4.8 cm/sec, an initial vortex separation of 13.4 cm, and $N = 0.33$ gives a vortex Froude number of

$$F_r = U/Nb_0 = 1.1 \quad .$$

Figure 24 shows the data in Figure 23 replotted with data from Sarpkaya (1983) for a similar Froude number. Figure 24 shows that our data is consistent with data from previous investigations. This consistency means that our technique of using the starting vortices from wings is a credible method of producing a vortex pair.

Figure 25 shows vortex evolution in a stratified sheared flow. This figure shows streak photographs of the flow at several times after vortex generation. The streaks result from a time exposure of neutrally buoyant particles. In this run, $N = 0.33$ sec^{-1} and $U_z = 0.39$ sec^{-1}, resulting in a Richardson number of 0.73. The shear is from left to right at the top of the photograph and from right to left at the bottom of the photograph, resulting in a clockwise rotation of the mean shear. In Figure 25, the first few photographs show a symmetric evolution, with the left and right vortices showing nearly the same rise and strength. After a short while, however, the left vortex, which has a rotational sense opposite that of the mean shear, begins to decay and finally disappears altogether, leaving only the right vortex. This remaining, solitary vortex continues to persist until surges from the end walls change the flow conditions.

To quantify the effects of the shear, we measured the circulation of the vortices as a function of time, in a manner similar to that in Delisi et al (1991). Circulation results for nonstratified, nonsheared runs are shown in Figure 26. This figure shows that the circulations of the left and right vortices are nearly equal, as expected. Figure 27 shows the corresponding circulations for the stratified, nonsheared runs. Note that the circulations for these runs are nearly identical to those for the nonstratified runs, which is expected at early times. At later times, when the stratification effects become important, the circulations in the stratified runs should be lower than those in the nonstratified runs due to energy going into the internal wave field. This effect is not shown in Figure 26 since the nonstratified vortices approach the top of the tank quickly.

Figure 28 shows the vortex circulations for selected stratified, sheared runs. The importance of this figure is that it shows how, in high-Richardson-number flows, the vortices resemble vortices in nonsheared flows, but that the vortices look different in low-Richardson-number (high shear) flows.
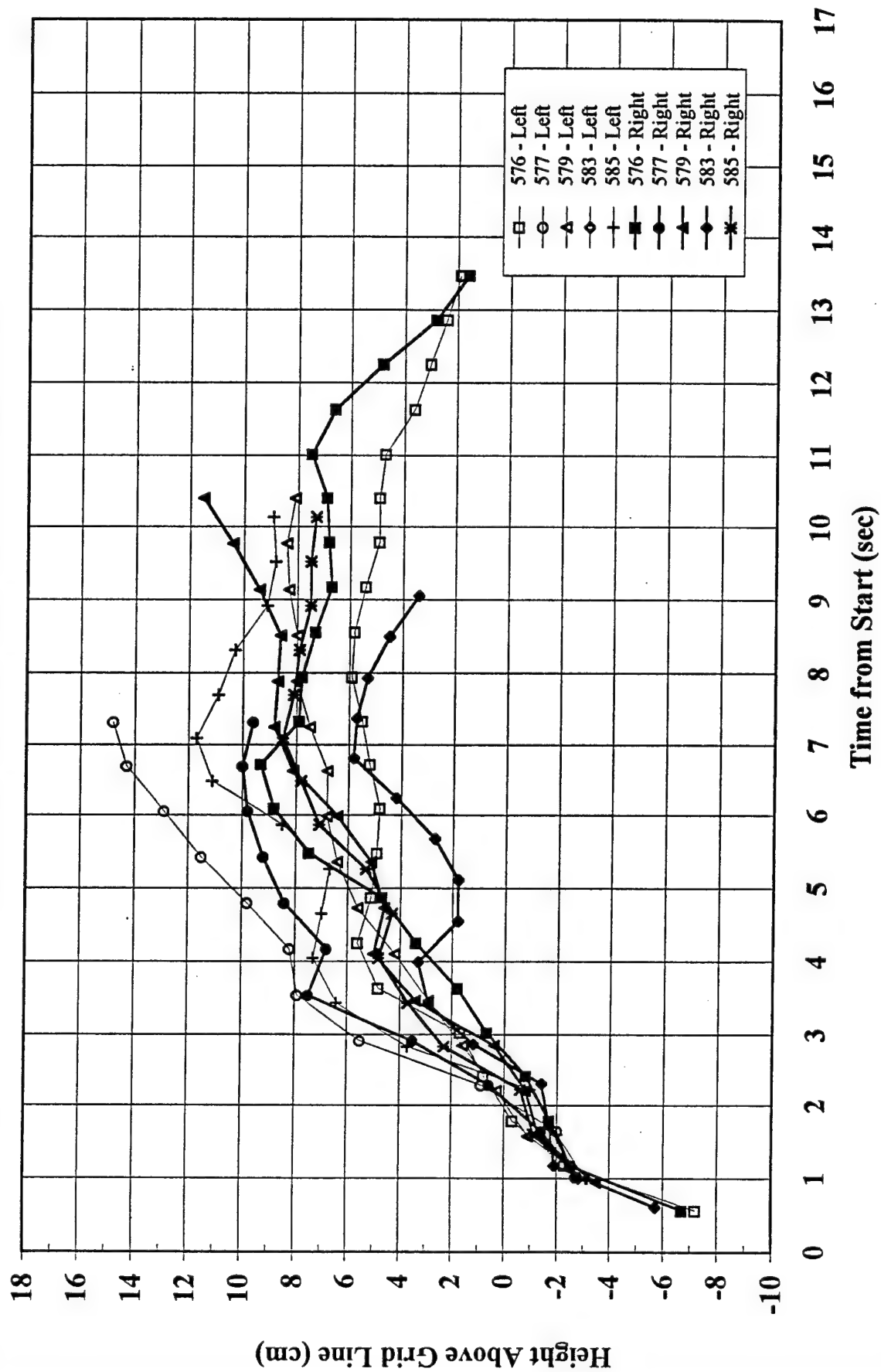
Figure 22.   Depth vs time for vortices from five nominally identical runs in the tilt tank with N = 0.33 sec^{-1} and no shear.

37
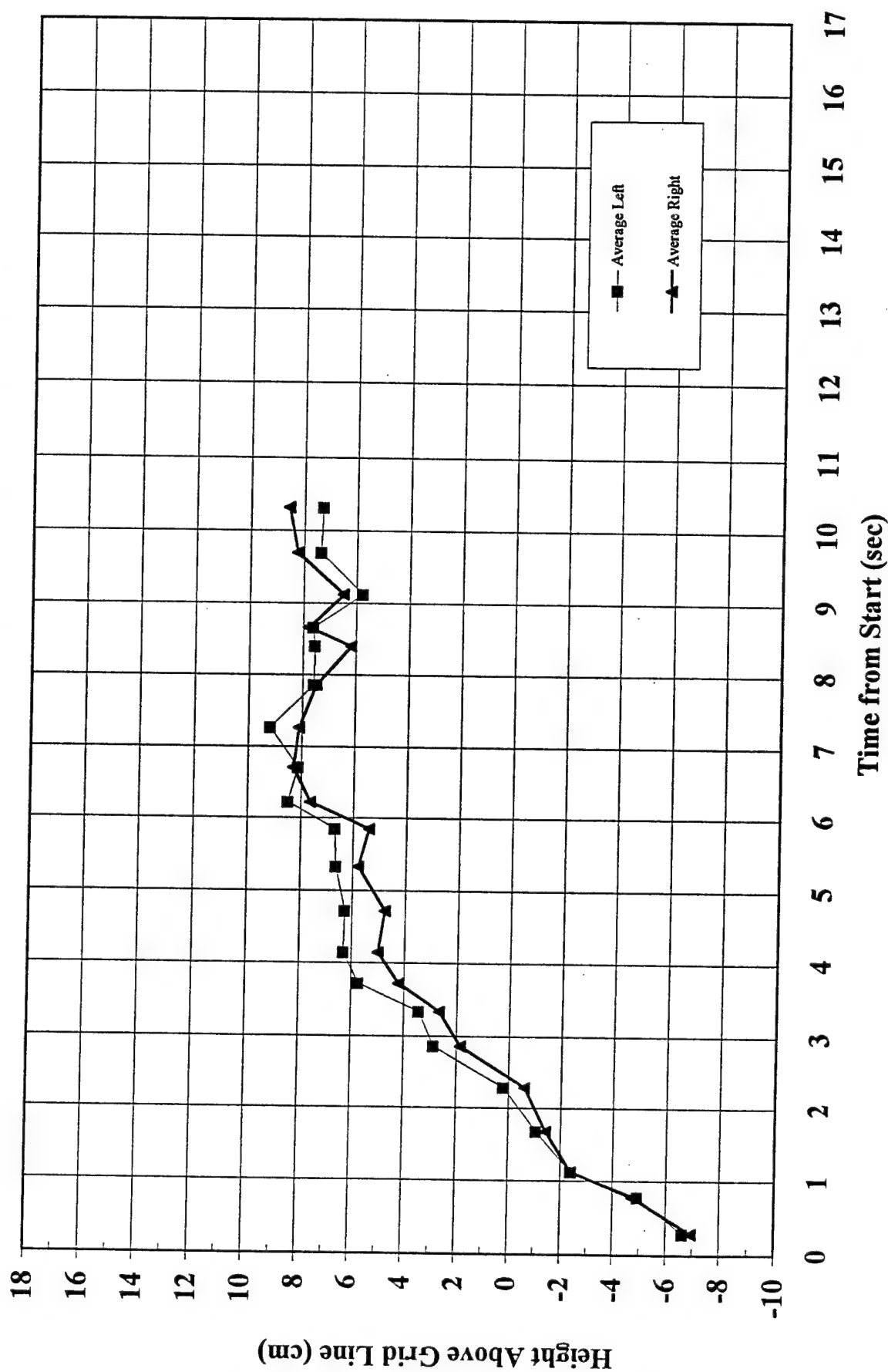
Figure 23. The average of the data shown in Figure 22.
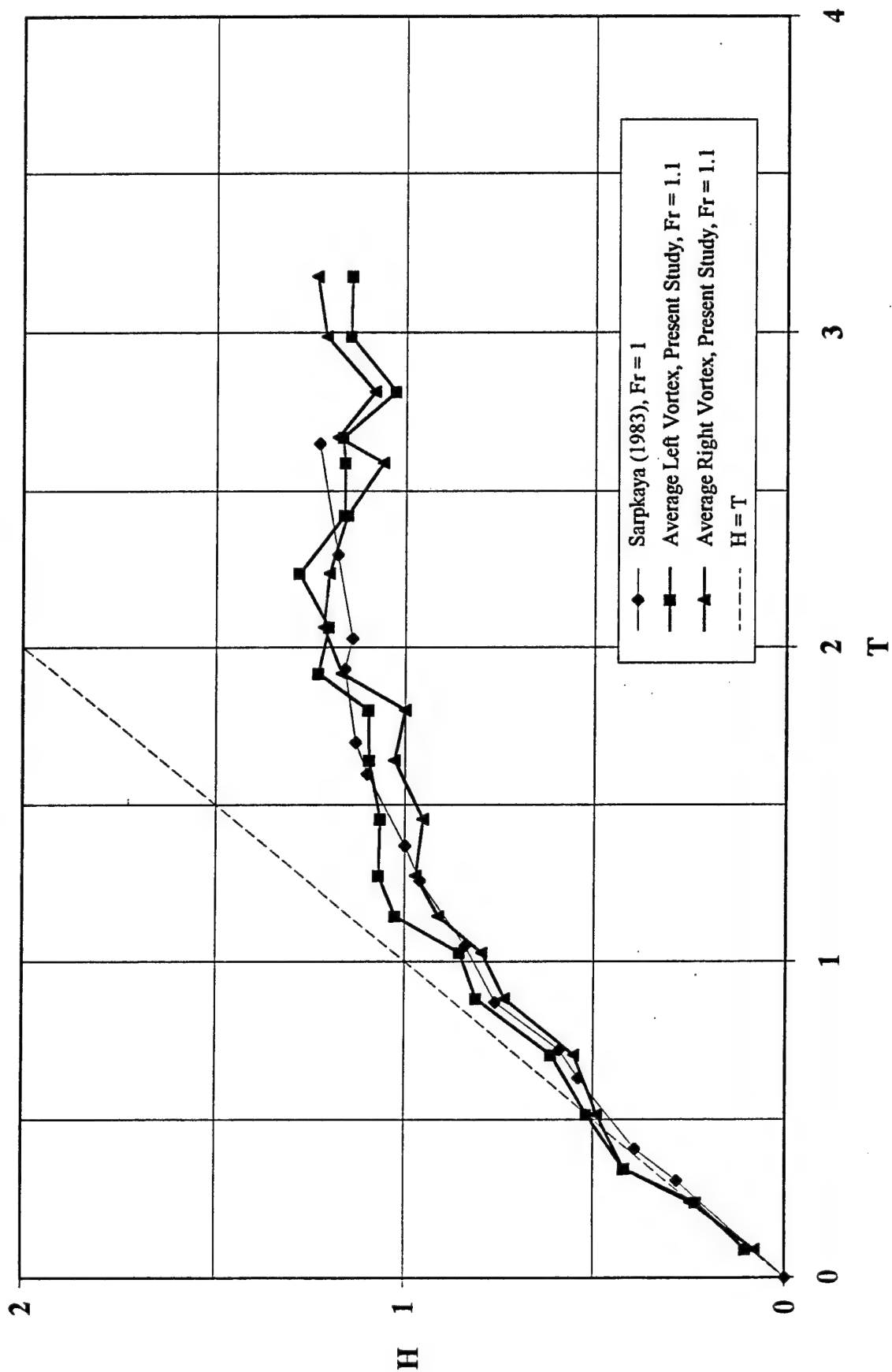
Figure 24. The data shown in Figure 23 plotted with the data from Sarpkaya (1983), $F_r = 1$.
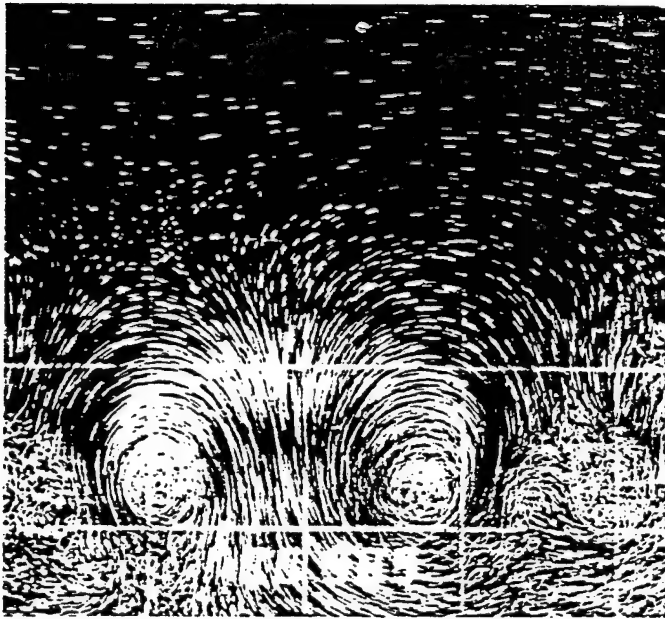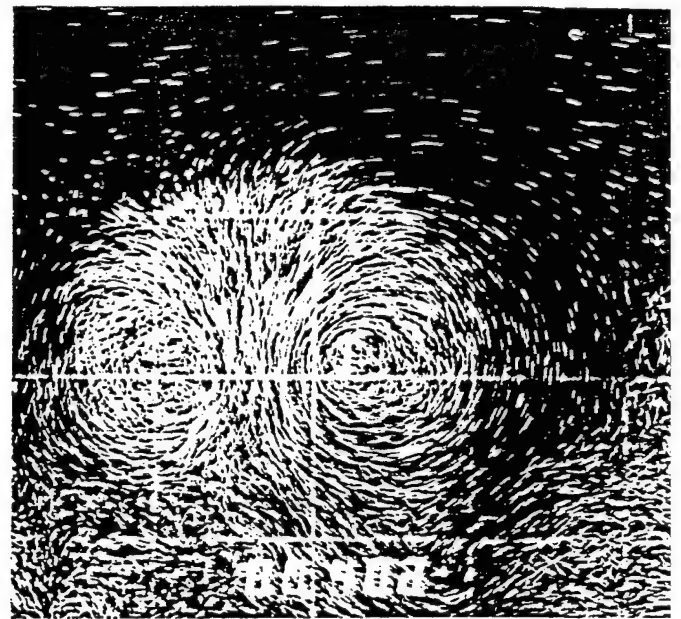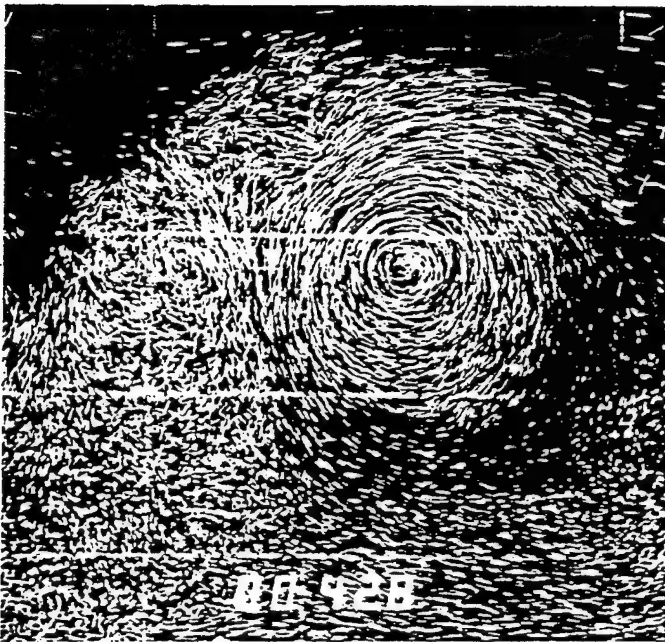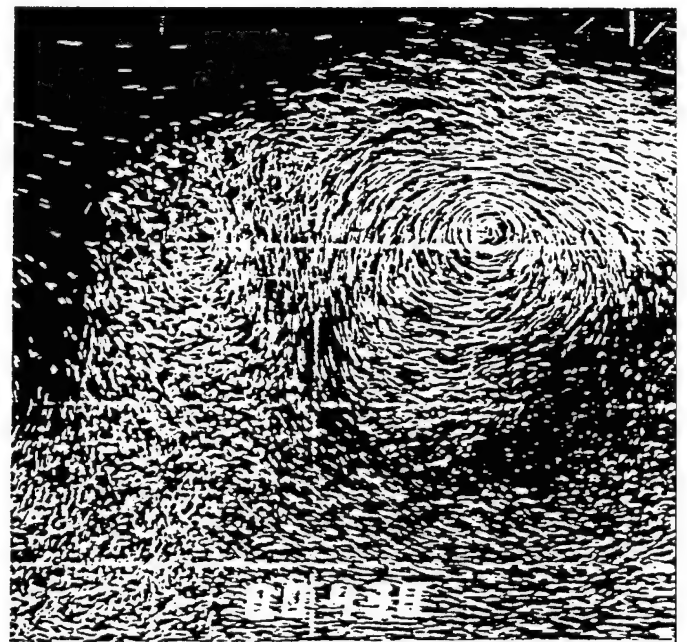
Figure 25.   Streak photographs showing vortex evolution in a stratified shear flow with Ri = 0.73.

Circulation for Nonstratified, Nonsheared Runs
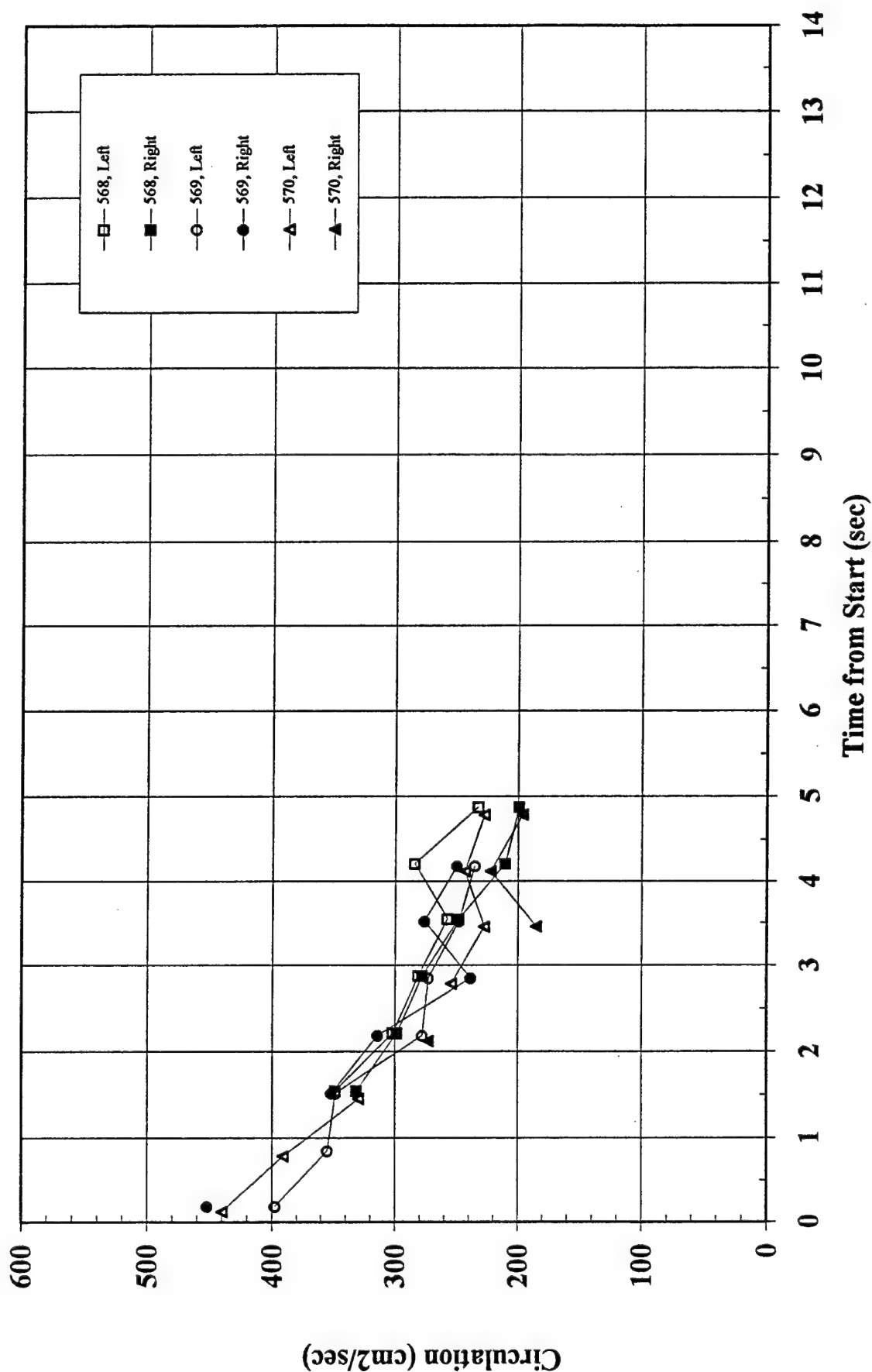
Figure 26.   Circulation vs time for the nonstratified, nonsheared runs.

41

Circulation for Stratified, Nonsheared Runs
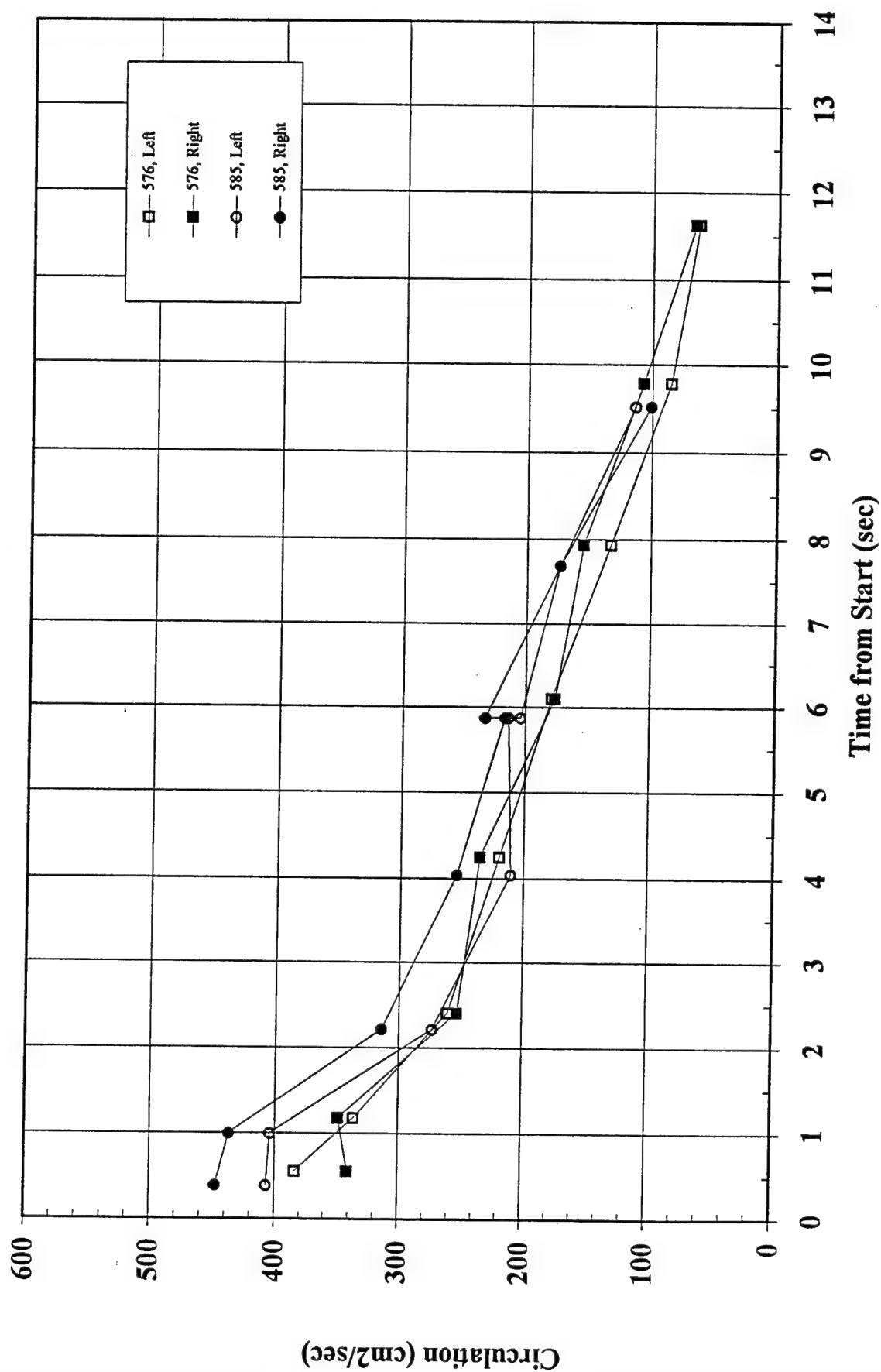
Figure 27.   Circulation vs time for the stratified, nonsheared runs.

42

Circulation for Stratified, Sheared Runs
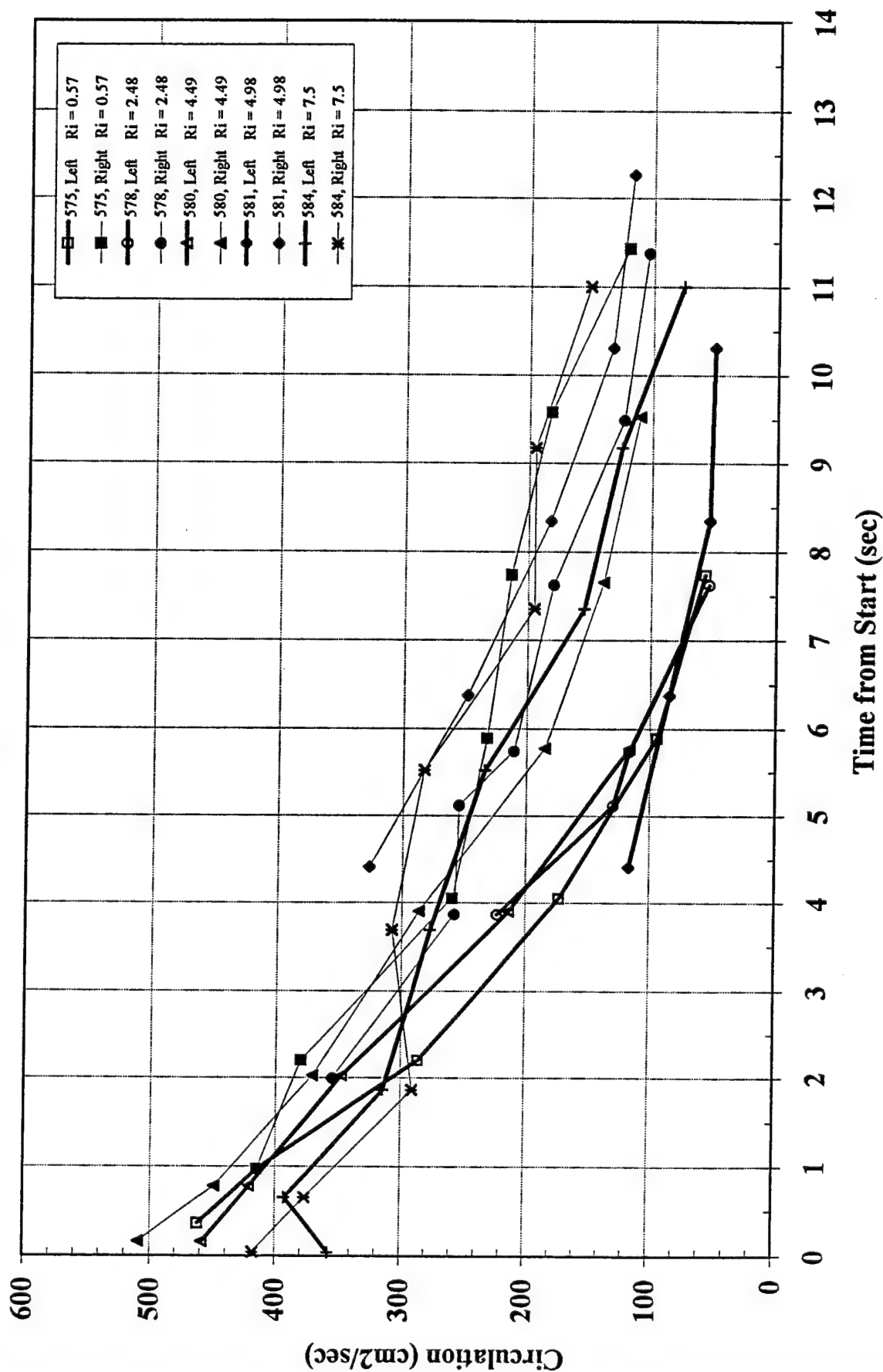
Figure 28. Circulation *vs* time for the stratified, sheared runs. Left vortex values have been connected with thicker lines to distinguish them from the right vortex values. Note that the left vortices decay faster than the right vortices in low Richardson number flows (cf., Figures 5, 6, 9, 10, 14, 15, and 25).

43

4.5. Additional Numerical Work

In Robins and Delisi (1990, 1993) and Delisi et al (1991), we modeled vortex pairs using a numerical model which included a scale-dependent viscosity to control numerical instability and to provide a mechanism for the dissipation of any energy that was transferred from larger to smaller scales. This technique provided results that compared well with laboratory and field measurements of trajectories of trailing vortices evolving for short times in nonstratified nonsheared flows, stratified nonsheared flows, and stratified sheared flows. By short times, we mean times $\leq 5T_0$ where T_0 is the time required for the vortices to move vertically an amount equal to their separation distance. Symbolically,

$$T_0 = b_0 / V_0 \quad . \tag{5}$$

V_0 can be expressed approximately in terms of the circulation, Γ_0, around each of the vortices as

$$V_0 = \Gamma_0 / 2\pi b_0 \quad . \tag{6}$$

For point vortices, this expression is exact. In turn, Γ_0 can be related to the lift forces which cause the vortices to form.

We have found that, for times on the order of $10T_0$, the above model overpredicts the rise of vortices observed in laboratory nonstratified, nonsheared flows. This result is shown by the curve labeled $C_\mu = 0.0$ in Figure 29. We also noted that our model did not dissipate circulation as rapidly as was observed. [This difficulty is evident from Figure 15 and Figures 2 and 8 in Robins and Delisi (1993)]. Since it was clear from viewing the laboratory experiments that the vortices were turbulent, we hypothesized that one reason for the discrepancies was that the dissipation mechanism in our numerical model did not adequately represent the effects of turbulence. Encouraged by examples from Rodi (1984, 1987), we proceeded to try using a k-ε model to improve our treatment of turbulent dissipation.

Our k-ε model solves equations for the following dependent variables: $\overline{\eta}$, the mean vorticity; $\overline{\rho}$, the mean density; k, the turbulent kinetic energy; and ε, the dissipation rate of k. The equations for $\overline{\eta}$ and $\overline{\rho}$ were derived from the 2-D Navier-Stokes equations for an incompressible fluid to which the Boussinesq approximation[1] was applied. We started with equations for horizontal velocity, v, vertical velocity, w, and density, ρ, and then obtained the model equations by representing each dependent variable as a sum of background, mean, and fluctuating components. Background quantities were assumed to be geophysically imposed, and the mean quantities were defined as averages over long times compared to the time scales of the fluctuations. The equations for k and ε are based on the k-ε turbulence model described by Rodi (1984), which we reformulated in terms of vorticity and density.

---

[1]Variations of density in the momentum equations are neglected except when they give rise to buoyancy forces.
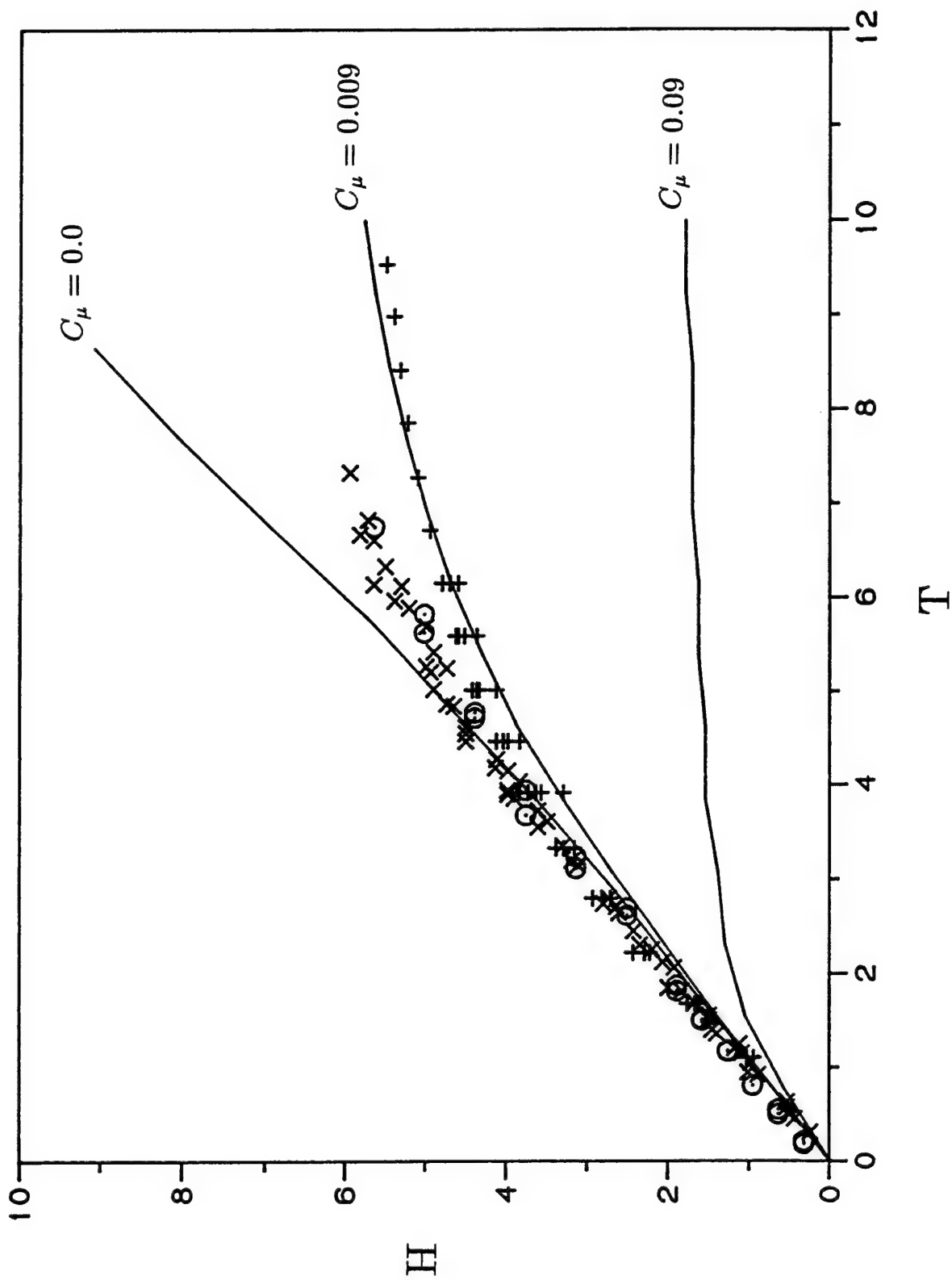
44

Figure 29. Lab measurements and computer simulations of H vs T for vortex rise in nonstratified, nonsheared fluids. Data from Delisi and Greene (1990), Sarpkaya (1983), and Tomassian (1979) are shown by •, ×, and +, respectively. Computer results for three values of C_μ are shown by solid lines.

In order to solve the four equations for $\bar{\eta}$, $\bar{\rho}$, k, and ε, we adopted the following approach: all horizontal derivatives are computed using fast Fourier transforms, all vertical derivatives are computed by second-order centered differences, and time is advanced using the third-order Adams-Bashforth method (Durran, 1991). Free slip conditions are imposed at the top and bottom boundaries of the computational domain, and periodicity is ensured at the side boundaries. The two-thirds rule (Canuto et al, 1988) is used to avoid aliasing error from the computation of horizontal derivatives, and a cosine-squared taper is applied to the upper ten percent of the unaliased spectrum to prevent build-up of small-scale numerical noise.

The initial vorticity is specified as a pair of counter-rotating Gaussian vortices as described in Robins and Delisi (1990), and the initial turbulent kinetic energy is given a Gaussian distribution spatially coincident with the initial vorticity. Following Lewellen (1977) and Hecht et al (1980), we set the initial dissipation rate to

$$\varepsilon = 0.35 k^{3/2} / L \; , \tag{7}$$

where L is the macroscale of the turbulent eddies, which we assume equal to the core radius of the initial vortices. Time-independent, background-density, and current profiles are specified, and we assume there is no vortex-induced initial density deviation from the background state.

The ambient turbulent kinetic energy is determined from an estimate of $f = \nu_T / \nu_M$ (where ν_T is the eddy viscosity, and ν_M is the molecular viscosity), in conjunction with the above expression for ε and the defining expression for eddy viscosity,

$$\nu_T = C_\mu k^2 / \varepsilon \; , \tag{8}$$

where C_μ is the primary turbulence model constant. Namely,

$$k_{AMB} = (0.35 f \nu_M / C_\mu L)^2 \; . \tag{9}$$

The turbulent kinetic energy at the center of the vortices is arbitrarily taken to be one hundred times the ambient value, an estimate supported by the examination of the field measurements of Burnham et al (1978) and the numerical results of Hecht et al (1980). As the calculation proceeds, the turbulent kinetic energy is never allowed to go below its ambient value.

In the following three examples, the core radius of the computer-simulated vortices is taken to be twenty percent of the separation distance. In the first two cases, the ambient eddy viscosity is taken equal to the molecular viscosity, and in the third case it is taken to be five times the molecular viscosity.

The first case is vortex migration in a nonstratified, nonsheared fluid. Figure 29 is a repeat of Figure 11 with the addition of numerical results for three values of C_μ. The computed result

46

for $C_\mu = 0.0$ is from the code described in Robins and Delisi (1990), and the result for $C_\mu = 0.09$ is from the code described above. This value for C_μ is the standard model value, based on lab data for parallel flow past a flat surface. Figure 29 clearly shows that the code severely under-predicts the vortex migration when this standard value for C_μ is used. However, when C_μ is chosen to be 0.009, the agreement between code results and data is quite good. This choice for C_μ was motivated by the following comment from the introduction to Bradshaw's monograph on curved flow (1973), "...it is helpful to recognize that streamline curvature is not an isolated pathological case but one of a group of distortions ('extra rates of strain') which produce unexpectedly large effects on turbulent shear layers. By the words 'surprisingly' and 'unexpectedly' we imply that the effects of extra rates of strain are an order of magnitude larger than would be predicted by straightforward extensions of calculation methods for simple shear layers."

An interesting aspect of the code/data comparisons for $C_\mu = 0.009$ stems from the observation that the data of Delisi and Greene and of Sarpkaya were for 3-D trailing vortices, while the data of Tomassian were for 2-D vortices from a vortex generator. It might only be coincidental, but the 2-D code results agree best with the 2-D data.

The second case is vortex migration in a stratified, nonsheared fluid. All calculation parameters for this case are the same as for the first case (with $C_\mu = 0.009$), except for the addition of background stratification. The results for this case are summarized in Figure 30, which shows lab data from Liu and Smsky (1990), Tomassian (1979), and Sarpkaya (1983), for Froude numbers 1.97, 2.00, and 1.00, respectively. The agreement between code results and data is seen to be reasonably good.

Figure 31 shows results for vortex evolution in a stratified, sheared fluid, for which the Richardson number is 1.0. This figure, without the results for $C_\mu = 0.009$, appears as Figure 15 of this report. It can be seen that the code using the turbulence model with $C_\mu = 0.009$ does a better job of simulating circulation history than the result (shown here and in Figure 15) for $C_\mu = 0.0$.

In summary, evidently (and not surprisingly) the standard k-ε turbulence model does a poor job of representing the turbulent dissipation in highly curved flows such as found in trailing vortices. The curvature of the flow apparently suppresses dissipation due to turbulence, an effect which we were able to model by a suitable reduction in the eddy viscosity coefficient. This approach does not pretend to accurately describe the complicated fluid physics occurring in trailing vortex flows but does seem to permit the simulation of gross flow characteristics such as the migration trajectory and the circulation history.
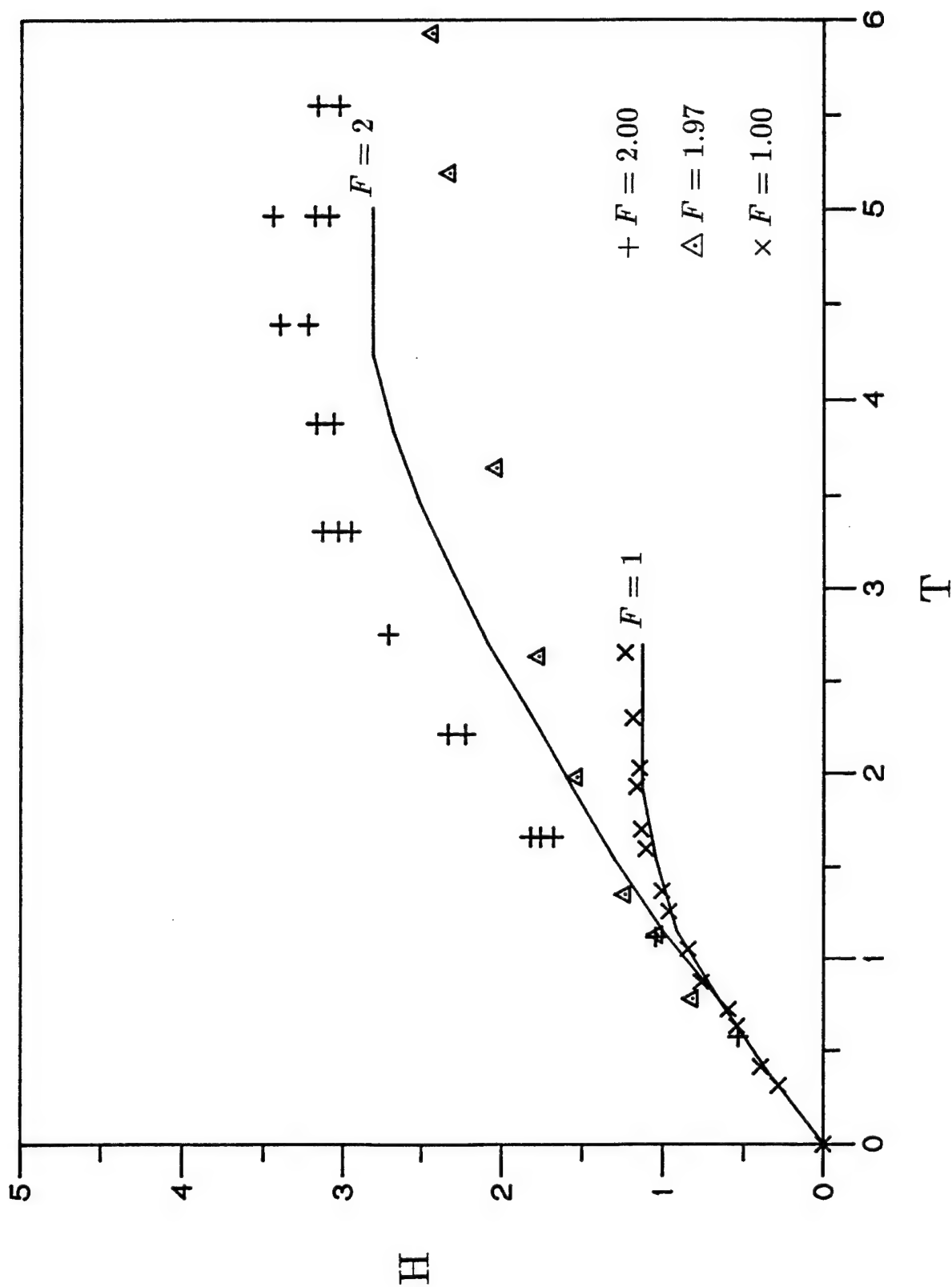
Figure 30. Lab measurements and computer simulations of H vs T for vortex rise in stratified, nonsheared fluids. Data of Sarpkaya (1983), Tomassian (1979), and Liu and Srnsky (1990) are shown by ×, +, and •, respectively. Computer results for two values of Froude number are shown by solid lines.
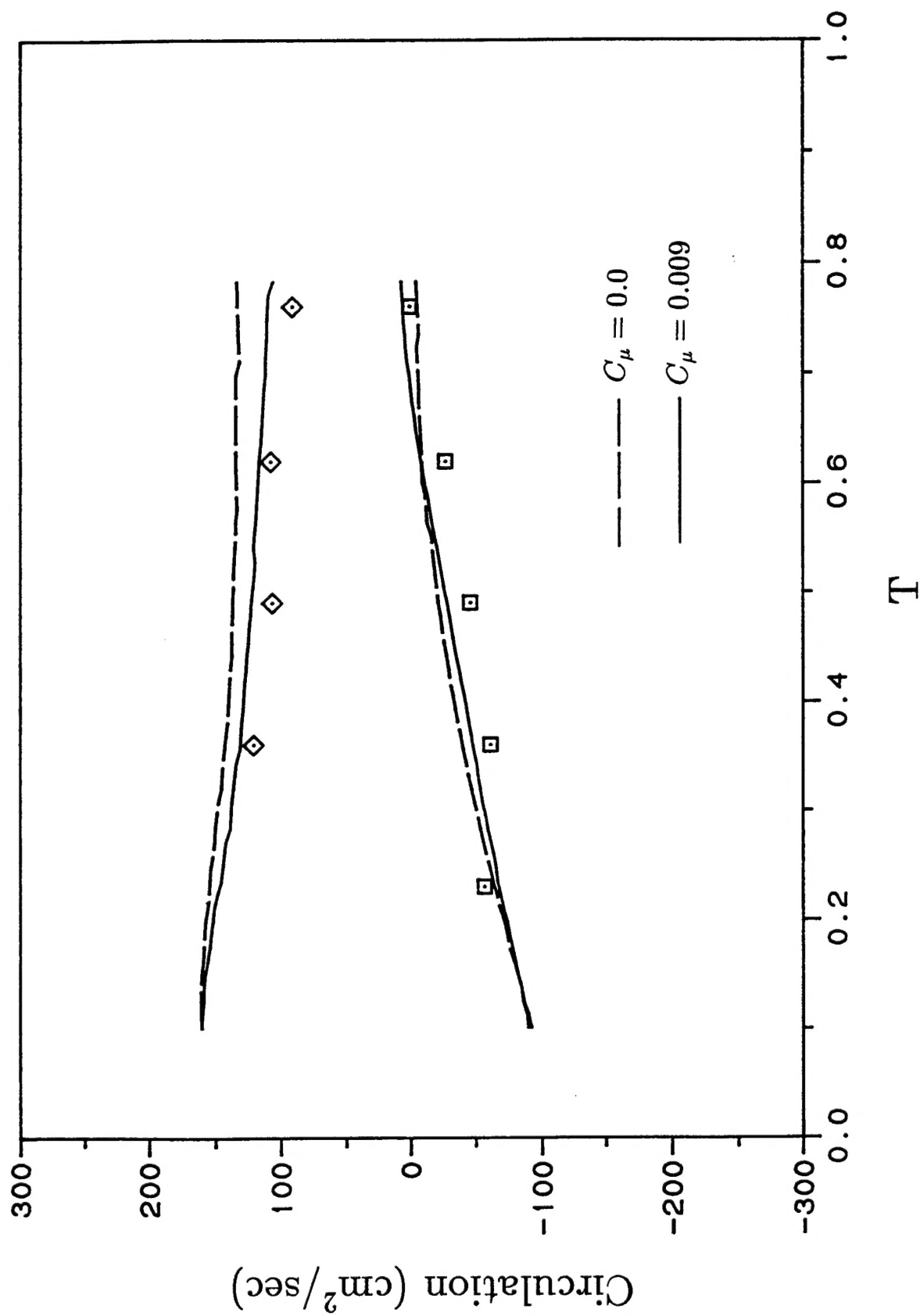
Figure 31. Circulation vs T for a laboratory case and two computer simulations. The laboratory data and the $C_\mu = 0.0$ simulation are from Figure 15. The $C_\mu = 0.009$ simulation results are from the model described in Section 4.5.

49

5.   Comments

This report describes laboratory experiments and numerical simulations which were performed to investigate vortex dynamics in realistic flows. Additional laboratory and numerical studies are currently underway and will be reported on later.

References

Barker, S.J., and Crow, S.C., 1977. The Motion of Two-Dimensional Vortex Pairs in a Ground Effect. *J. Fluid Mechanics, 82*, 659-671.

Bilanin, A.J., Teske, M.E., and Hirsch, J.E., 1978. Neutral Atmospheric Effects on the Dissipation of Aircraft Vortex Wakes. *AIAA Journal, 16*, 956-961.

Bradshaw, P., 1973. Effects of Streamline Curvature on Turbulent Flow. AGARDograph No. 169.

Burnham, D.C., Hallock, J.N., Tombach, I.H., Brashears, M.R., and Barber, M.R., 1978. Ground-Based Measurements of the Wake Vortex Characteristics of a B-747 Aircraft in Various Configurations. U.S. Dept. of Trans., FAA Report DOT-TSC-FAA-78-28.

Canuto, C., Hussaini, M.Y., Quarteroni, A., and Zang, T.A., 1988. *Spectral Methods in Fluid Dynamics.* Springer-Verlag, New York.

Crow, S.C., 1970. Stability Theory for a Pair of Trailing Vortices. *AIAA Journal, 8*, 2172-2179.

Delisi, D.P., Robins, R.E., and Lucas, R.D., 1991.   Initial Laboratory Observations of the Evolution of a Vortex Pair in a Stratified Shear Flow. *Phys. Fluids A, 3*, 2489-2491.

Delisi, D.P., and Greene, G.C., 1990. Measurements and Implications of Vortex Motions Using Two Flow-Visualization Techniques. *J. Aircraft, 27*, 968-971.

Durran, D.R., 1991. The Third-Order Adams-Bashforth Method: An Attractive Alternative to Leapfrog Time Differencing. *Mon. Wea. Rev., 119*, 702-720.

Greene, G.C., 1986. An Approximate Model of Vortex Decay in the Atmosphere. *J. Aircraft, 23*, 566-573.

Evans, D.L., 1982. Observations of Small-Scale Shear and Density Structure in the Ocean. *Deep-Sea Res., 29*, 581-595.

Hall, M.G., 1972. Vortex Breakdown. *Annual Reviews of Fluid Mechanics, 4*, 195-218.

Hecht, A.M., Hirsh, J.E., and Bilanin, A.J., 1980. Turbulent Trailing Vortices in Stratified Fluids. AIAA Paper No. 80-0009, Presented at the 18th AIAA Aerospace Sciences Meeting, January 14-16.

Leibovich, S., 1978. The Structure of Vortex Breakdown. *Annual Reviews of Fluid Mechanics, 10*, 221-246.

Lewellen, W.S., 1977. Use of Invariant Modeling. Chap. 9 in *Handbook of Turbulence, Vol. 1* (ed. W. Frost and T.H. Moulden). Plenum, New York.

Liu, H.-T., and Srnsky, R.A., 1990. Laboratory Investigation of Atmospheric Effects on Vortex Wakes. Flow Technical Report No. 497, Kent, WA.

Robins, R.E., and Delisi, D.P., 1990. Numerical Study of Vertical Shear and Stratification Effects on the Evolution of a Vortex Pair. *AIAA Journal, 28*, 661-669.

Robins, R.E., and Delisi, D.P., 1993. The Potential Hazard of Aircraft Wake Vortices in Ground Effect with Crosswind. *J. Aircraft, 30*, 201-206.

Rodi, W., 1984. *Turbulence Models and Their Application in Hydraulics.* International Association for Hydraulic Research, Delft, Netherlands.

Rodi, W., 1987. Examples of Calculation Methods for Flow and Mixing in Stratified Fluids. *J. Geophys. Res., 92*, C5, 5305-5328.

Saffman, P.G., and Baker, G.R., 1979. Vortex Interactions. *Annual Reviews of Fluid Mechanics, 11*, 95-122.

Sarpkaya, T., 1983. Trailing Vortices in Homogeneous and Density-Stratified Media. *J. Fluid Mech., 136*, 85-109.

Sarpkaya, T., 1989. Computational Methods With Vortices - The 1988 Freeman Scholar Lecture. *J. Fluids Engineering, 111*, 5-52.

Sarpkaya, T., and S.K. Johnson, 1982. "Trailing Vortices in Stratified Fluids," Naval Postgraduate School, Monterey, CA, Rept NPS-69-82-003.

Scorer, R.S., 1958. *Natural Aerodynamics.* Pergamon Press, New York.

Smith, J.H.B., 1986. Vortex Flows in Aerodynamics. *Annual Reviews of Fluid Mechanics, 18,* 221-242.

Thorpe, S.A., 1968. A Method of Producing Shear Flow in a Stratified Fluid. *J. Fluid Mech., 32,* 693-704.

Thorpe, S.A., 1969. Experiments on the Instability of Stratified Shear Flows: Immisible Fluids. *J. Fluid Mech., 39,* 25-48.

Thorpe, S.A., 1985. Laboratory Observations of Secondary Structures in Kelvin-Helmholtz Billows and Consequences for Ocean Mixing. *Geophys. Astrophys. Fluid Dyn., 34,* 175-199.

Tomassian, J.D., 1979. The Motion of a Vortex Pair in a Stratified Medium. Ph. D. Thesis, University of California, Los Angeles, CA.

Toole, J.M., and Hayes, S.P., 1984. Finescale Velocity-Density Characteristics and Richardson Number Statistics of the Eastern Equatorial Pacific. *J. Phys. Oceanogr., 14,* 712-726.

Widnall, S.E., 1975. The Structure and Dynamics of Vortex Filaments. *Annual Reviews of Fluid Mechanics, 7,* 141-165.